Robust Multi-Robot Trajectory Generation Using Alternating Direction Method of Multiplier

Ruiqi Ni¹, Zherong Pan² and Xifeng Gao²

Abstract—We propose a variant of alternating direction method of multiplier (ADMM) to solve constrained trajectory optimization problems. Our ADMM framework breaks a joint optimization into small sub-problems, leading to a low iteration cost and decentralized parameter updates. Our method inherits the theoretical properties of primal interior point method (P-IPM), i.e., guaranteed collision avoidance and homotopy preservation, while being orders of magnitude faster. We have analyzed the convergence and evaluated our method for time-optimal multi-UAV trajectory optimizations and simultaneous goal-reaching of multiple robot arms, where we take into consider kinematics-, dynamics-limits, and homotopy-preserving collision constraints. Our method highlights $10-100\times$ speedup, while generating trajectories of comparable qualities as state-of-the-art P-IPM solver.

I. INTRODUCTION

This paper focuses on trajectory generation problems, a fundamental topic in robotic manipulation and control systems. Although the problem finds countless domains of applications, their pivotal common feature could be illustrated through the lens of two applications: multi-UAV trajectory planning & goal-reaching of articulated robot arms.

UAV trajectory planning has been studied vastly [1]. Due to their small size and differential-flat dynamics [2], point-mass models can be used and Cartesian-space trajectories are linear functions of configuration variables. Furthermore, the quality of a UAV trajectory could be measured via convex metrics such as jerk or snap, casting trajectory generation as convex programs. However, when flying in obstacle-rich environments and among other UAVs, non-convex, collision-free constraints must be considered [3]. Failing to satisfy these constraints can render a generated trajectory completely useless. Due to limited sensor range and uncertainties, however, collision-free constraints are not completely known to the planner. Thereby, a trajectory generator must get prepared to re-plan online based on updated environment information [4]. Handling articulated robot arms poses an even more challenging problem, where the linear dynamic assumption must be replaced with a nonlinear forward kinematic function that maps from configuration- to Cartesian-space, rendering all the Cartesian-space constraints non-convex. In summary, a trajectory generator should pertain three properties: (versatility) handle non-convex constraints and kinematic models; (robustness) guarantee to satisfy all the constraints throughout the execution; (efficacy) fast enough for frequent re-planning.

We focus on optimization-based trajectory generation methods. Alternative methods, such as anytime sampling-based roadmaps [5], control barrier functions [6], and navigation vector fields [7], exhibit remarkable performs under certain assumptions but have partial coverage of the three features above. Sampling-based methods, for example, have good versatility and robustness but they are sample-intensive and less efficient. Control barrier functions and navigation vector fields are constructed based on simple or known environments,

so they are less suitable for online applications. In our prior work [8], we proposed a new underlying solver for UAV trajectory planning with perfect versatility and robustness. Ni et al. [8] converts all the constraints into primal-only logbarrier functions with finite duality gap. As a result, all the constraints are satisfied throughout the optimization. With the improved robustness, however, comes a much inferior rate of convergence. For the same benchmarks, our primal-only methods can take $3-5\times$ more computations to converge as compared with primal-dual counterparts. This is due to the logbarrier functions introducing arbitrarily large gradients near the constraint boundaries. As a result, an optimizer needs to use a costly line-search after each iteration to ensure a safe solution that satisfies all the stiff constraints. The gradientflows of such objective functions are known as stiff dynamics, for which numerical time-integration can have ill-convergence as studied [9].

Main Results: We propose a variant of ADMM-type solver that inherits the versatility and robustness from [8], while we achieve orders of magnitude higher performance. Intuitively, ADMM separates non-stiff and stiff objective terms into different sub-problems using slack variables, so that each subproblem is well-conditioned. Moreover, since sub-problems are independent and involve very few decision variables, an ADMM iteration can be trivially parallelized and incurs a much lower cost. Existing convergence analysis, however, only guarantees that ADMM converges for convex problems or non-convex problems with linear constraints. We present improved analysis which shows that our ADMM variant converges for both UAV and articulated trajectory planning problems under nonlinear collision-free constraints, kinematicand dynamic-limits. We have applied our method to largescale multi-UAV trajectory generations and articulated multirobot goal-reaching problems as defined in Section III. During our evaluations (Section V), we observe $10 - 100 \times$ speedup over Newton-type methods. Our algorithms are detailed in Section IV.

II. RELATED WORK

We compare our method with other trajectory generators and cover necessary backgrounds in operations research.

Trajectory Generation aims at computing the control signals to realize a given motion. Their typical scenarios of applications involve navigation [7], multi-UAV coordination [10], human-robot interaction [11], tele-operations [12], etc., where frequent trajectory update is a necessity to handle various sources of uncertainty. Due to the limited computational resources, early works use pre-computations to reduce the runtime cost. For example, Panagou, Shimoda *et al.* [7, 13] modulate a vector field to guide agents in a collision free manner, while assuming point robots and known environments. Closed-form solutions such as [14, 15] exists but are limited to certain types of dynamic systems or problem paradigms. More recently, Belghith *et al.*, Karaman *et al.* [5, 16] have established anytime-variants of sampling-based roadmaps that continually improve an initial feasible solution

Department of Computer Science, Florida State University, rn19g@my.fsu.edu. ² Lightspeed & Quantum Studio, Tencent America, {zherong.pan.usa, gxf.xisha}@gmail.com.

during execution. These methods inherit the generality of sampling-based roadmaps but they tend to be sample-intensive in higher-dimensional configuration spaces. Finally, contact-aware trajectory generation [17] has emerged as an independent direction of research that focuses on the joint planning of robot poses and contact configurations, but handling contacts is beyond the scope of our research.

Trajectory Optimization dates back to [18, 19], but has recently gained significantly attention due to their superior versatility and the maturity of nonlinear programming solvers. These methods have robots' goal of navigation formulated as objective functions, while taking various safety requirements as (non)linear constraints. They achieve unprecedented success in real-time control of high-dimensional articulated bodies [20] and large swarms of UAVs [3]. On the down side, trajectory optimization suffers from a lack of guarantee. Many works formulate constraints as soft objective functions [21, 20] or use primal-dual interior point methods to handle non-convex constraints [22, 19, 23], which does not guarantee constraint satisfaction. On the other hand, some techniques [24, 25] restrict the solution space to a disjoint convex subset so that efficient solvers are available, but these methods are limited to returning sub-optimal solutions. Instead, Ni et al. [8] use primal-only methods and transform non-convex constraints into log-barrier functions with finite duality gap, so that constraint satisfaction is guarantee and no restrictions in solution space are needed. But optimizer in this case can make slow progress, being blocked by the large gradient of log-barrier functions. This dilemma between efficacy and robustness has been studied as stiff dynamic systems [9], for which dedicated techniques are developed for different applications such as numerical continuation [26]. Unlike these methods, we show that first-order methods can be combined with barrier methods to achieve significant speedup.

Alternating Direction Method of Multiplier is a firstorder optimization framework originally designed in convexprogramming paradigm [27]. ADMM features a low iteration cost and moderate accuracy of solutions, making it a stellar fit for online trajectory generations where many iterations can be performed within a short period of time. ADMM uses slack variables to split the problem into small subproblems and approximately maintains the consistency between slack and original variables by updating the Lagrangian multipliers. Although theoretical convergence guarantee was only available under convex assumptions, ADMM has been adapted to solve non-linear fluid dynamics control [28], collision-free UAV trajectory generation [29], and bipedal locomotion [30], where good empirically performances have been observed. It was not until very recently that the good performances of ADMM in nonlinear settings have been theoretically explained by [31, 32, 33]. Unfortunately, even these latest analysis cannot cover many robotic applications such as [29]. Our new ADMM algorithm correctly divides the responsibility between the slack and original variables, where the slack variables handle nonstiff function terms and the original variables handle stiff ones. By using line-search to ensure strict function decrease, we can prove convergence (speed) of our algorithm to a robust solution.

III. TRAJECTORY OPTIMIZATION PARADIGM

We motivate our analysis using a collision-free trajectory optimization problem as illustrated in Figure 1. Consider a point robot traveling in a 2D workspace along a piecewise linear trajectory discretized using N+1 linear segments and N+2 vertices. We further assume the start and goal positions are fixed, leaving the intermediary N points as decision variables. This trajectory can be parameterized by a vector $x \in \mathbb{R}^{2N}$ where $x_i \in \mathbb{R}^2$ is the *i*th vertex. For simplicity in this example,

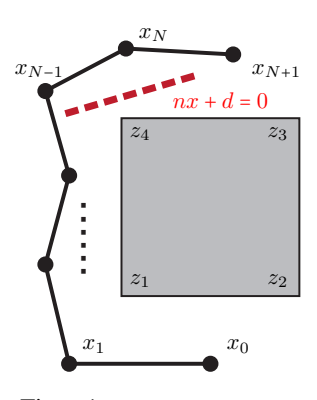


Fig. 1: Illustrative trajectory optimization problem. The red dashed line is the separating plane.

our goal is for the trajectory to be as smooth as possible. Further, the robot must be collision-free and cannot intersect the box-shaped obstacle in the middle and we assume that the four vertices of the box are $Z = \{z_1, z_2, z_3, z_4\}$. These collision-free constraints can be expressed as:

$$d(\text{hull}(X_i), \text{hull}(Z)) \ge 0 \quad \forall i = 1, \dots, N-1,$$

where $X_i = \{x_i, x_{i+1}\}$ is the *i*th line segment, hull (\bullet) denotes the convex hull and d is Euclidean the distance between two convex objects. A collision-free trajectory optimization problem can be formulated as:

$$\underset{x}{\operatorname{argmin}} \quad \sum_{i} X_{i}^{T} L X_{i}$$
s.t. $d(\operatorname{hull}(X_{i}), \operatorname{hull}(Z)) \ge 0 \quad \forall i = 1, \dots, N-1,$

where L is the Laplacian stencil measuring smoothness and $X_i^T L X_i$ measures the squared length of ith line segment. However, Equation 1 only considers geometric or kinematic constraints and a robot might not be able to traverse the optimized trajectory due to the violation physical constraints. In many problems, including autonomous driving [34] and UAV path planning [35], a simplified physical model can be incorporated that only considers velocity and acceleration limits. We could approximate the velocity and acceleration using finite-difference as:

$$V_i \triangleq x_{i+1} - x_i$$
 $A_i \triangleq x_{i+2} - 2x_{i+1} + x_i$,

and formulate the time-optimal, collision-free trajectory optimization problem as:

where we use $\sum_i X_i^T L X_i/\Delta t^2$ to measure trajectory smoothness with time, for example Dirichlet energy, and we use a coefficient w to balance between optimality in terms of trajectory length and arrival time. Here, v, a_{\max} are the upper bounds of velocities and accelerations. Although the above example is only considering a single robot and piecewise linear

trajectories, extensions to several practical problem settings are straightforward, as discussed below.

A. Time-Optimal Multi-UAV Path Planning

We first extend our formulation to handle multiple UAV trajectories represented using composite Bézier curves with N pieces of order M. In this case, the decision variable x is a set of N(M-2)+3 control points or $x \in \mathbb{R}^{3(N(M-2)+3)}$ (note that the two neighboring curves share 3 control points to ensure second order continuity and we refer readers to [8] for more details). For the ith piece of Bézier curve, the velocity and acceleration are defined as:

$$X_i \triangleq \begin{pmatrix} x_{i(M-2)-M+3} \\ \vdots \\ x_{i(M-2)+3} \end{pmatrix} \quad V_i(s) \triangleq \dot{I}(s)X_i \quad A_i(s) \triangleq \ddot{I}(s)X_i,$$

where X_i are the M+1 control points of the ith Bézier curve piece, and I(s), $\dot{I}(s)$ and $\ddot{I}(s)$ are the Bézier curve's interpolation stencil for position, velocity and acceleration, respectively, with $s \in [0,1]$ being the natural parameter. It can be shown that $V_i(s), A_i(s)$ are also Bézier curves of orders M-1 and M-2, respectively. The velocity and acceleration limits must hold for every $s \in [0,1]$, for which a finite-dimensional approximation is to require all the control points of $\dot{I}(s)$ and $\ddot{I}(s)$ are bounded by $v_{\rm max}$ and $a_{\rm max}$. With a slight abuse of notation, we reuse I, \dot{I}, \ddot{I} without parameter s to denote the matrices extracting the control points of $I(s)X_i, \dot{I}(s)X_i, \ddot{I}(s)X_i$, respectively. In other words, the vectors $V_i = \dot{I}X_i$ and $A_i = \ddot{I}X_i$ are the control points of the ith Bézier curve, then the form of velocity and acceleration limits are identical to Equation 2.

For multiple UAVs, however, we need to consider the additional collision-free constraints between different trajectories. To further unify the notations, we concatenate the control points of different UAVs into a single vector x, i.e., two Bézier curve pieces might correspond to different UAVs, and we introduce collision-free constraints between different UAVs:

$$d(\text{hull}(X_i), \text{hull}(X_j)) \ge 0 \quad \forall i, j \in \text{different UAV}.$$

Our final formulation of time-optimal multi-UAV path planning takes the following form:

where we generalize the objective function with smoothness and time optimality to take an arbitrary, possibly non-convex form, $\mathcal{O}(X_i, \Delta t)$, which is a function of a single piece of sub-trajectory X_i . Almost all the objective functions in trajectory generation applications can be written in this form. For example, smoothness can be written as the sum of total curvature, snap, or jerk of each piece, and the end-point cost is only related to the last piece.

B. Trajectory Generation for Articulated Robot Arms

The position of UAV at any instance s on the ith Bézier curve is $A(s)X_i$, which is a linear function of decision

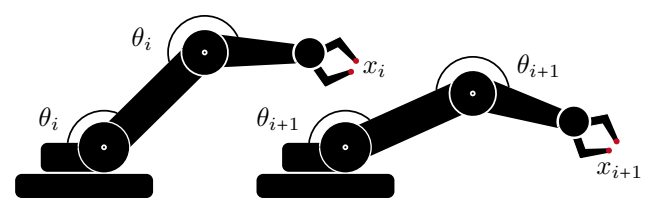


Fig. 2: We illustrate the nonlinear ADMM constraint due to an articulated robot arm. At each time instance, the configuration θ_i is related to the end-effector position x_i (red) (or any other position throughout the robot arm) via the forward kinematics function, which in turn defines the linear interpolated trajectory piece $X_i(\theta)$.

variable X_i and thus x. However, more general problem settings require non-linear relationships, of which a typical case is articulated robot arms. Consider the problem of multiple interacting robot arms in a shared 3D workspace. Each arm's Cartesian-space configuration at the ith time instance is represented by a triangle mesh with N vertices represented by x_i . However, we need to maintain the corresponding configuration θ_i , where $|\theta_i|$ is the degrees of freedom of each arm (DOF). Our decision variable is $\theta \in \mathbb{R}^{\mathrm{DOF} \times N}$ and each x_i is a derived variable of θ_i via the forward kinematics function $x_i \triangleq \mathrm{FK}(\theta_i)$ and a linear interpolated Cartesian-space trajectory is: $X_i(\theta) = \{x_i, x_{i+1}\} = \{FK(\theta_i), FK(\theta_{i+1})\}$. Therefore, the multi-arm trajectory generation problem can be formulated as:

$$\begin{aligned} & \underset{\theta, \Delta t}{\operatorname{argmin}} & \sum_{i} \mathcal{O}(X_{i}(\theta), \Delta t) \\ & \text{s.t. d}(\operatorname{hull}(X_{i}(\theta)), \operatorname{hull}(Z)) \geq 0 \quad \forall i = 1, \cdots, N-1 \\ & & \operatorname{d}(\operatorname{hull}(X_{i}(\theta)), \operatorname{hull}(X_{j}(\theta))) \geq 0 \quad \forall i, j \in \operatorname{different arm} \\ & \|V_{i}(\theta)\| \leq v_{\max} \Delta t \quad \forall i = 1, \cdots, N-1 \\ & \|A_{i}(\theta)\| \leq a_{\max} \Delta t^{2} \quad \forall i = 1, \cdots, N-2. \end{aligned}$$

Equation 4 takes a more general form than all the previous problems, and we would propose our variant of ADMM algorithm assuming this formulation. If our method is applied to UAV trajectory optimization, we can plug in the degenerate relationship $FK(\theta_i) = \theta_i$.

IV. ADMM-Type Trajectory Generation

ADMM is a variant of the Augmented Lagrangian Method (ALM) that does not update the penalty parameter. The main advantage of ADMM is that, by introducing slack variables, each substep of ADMM consists of either a small problem consisting of the non-stiff part of the objective function or a large problem consisting of the stiff part of the objective function or constraints. As a result, the ADMM solver allows larger timestep sizes to be taken for the non-stiff part, thus achieving faster convergence speed. Although ADMM has only first-order convergence speed, it can quickly approximate a locally optimal solution with moderate accuracy, which is sufficiently for trajectory generation problems.

ADMM handles inequality constraints by reformulating them as indicator functions, but we are handling possibly non-convex constraints for which projection operators, which is associated with indicator functions, do not have closed-form solutions. Instead, we follow our prior work [8] and rely on a log-barrier relaxations with non-zero duality gap. For example, if we have a hard constraint $g(x) \ge 0$ where g is some differentiable function, then the feasible domain can be identified with the finite sub-level set of the log-barrier function: $-\log(g(x))$. We apply this technique to the velocity

and acceleration limits. A similar technique can be used for collision-free constraints with the help of a separating plane, which is illustrated in Figure 1 as nx + d = 0 (n is the plane normal and d is the position). Since we only consider distance between convex hulls, two convex hulls are non-overlapping if and only if there is a separating plane such that the two hulls are on different sides. We propose to optimize the parameters of the separating plane (n,d) as additional slack variables. As a result, the collision constraints become convex when fixing n,d and optimizing the trajectory alone. Applying this idea to all the constraints and we can transform Equation 4 into the following unconstrained optimization:

$$\underset{\substack{\theta, \Delta t, d_i, d_{ij} \\ \|n_i\|, \|n_{ij}\| = 1}}{\operatorname{argmin}} \mathcal{L}(\theta, \Delta t, n_i, d_i, n_{ij}, d_{ij}) \triangleq \sum_{i} \mathcal{O}(X_i(\theta), \Delta t) - \sum_{i} \log(v_{\text{max}} \Delta t - \|V_i\|) - \gamma \sum_{i} \log(a_{\text{max}} \Delta t^2 - \|A_i\|) - \gamma \sum_{i} \left[\sum_{x \in X_i} \log(n_i x(\theta) + d_i) + \sum_{z \in Z} \log(-n_i z - d_i) \right] - \gamma \sum_{ij} \left[\sum_{x \in X_i} \log(n_i x(\theta) + d_{ij}) + \sum_{x \in X_j} \log(-n_i x(\theta) - d_{ij}) \right], \quad (5)$$

where γ is the weight of log-barrier function that can be tuned for each problem to control the exactness of constraint satisfaction.

Equation 5 is a strongly coupled problem with six sets of decision variables, where the constraints (or log-barrier functions) and the objective \mathcal{O} are added up. However, these two kinds of functions have very different properties. The log-barrier functions are "stiff" and do not have a Lipschitz constant, which could generate arbitrarily large blocking gradients near the constraint boundaries, but the objective \mathcal{O} is well-conditioned, oftentimes having a finite Lipschitz constant. Our main idea is to handle these functions in separate subproblems.

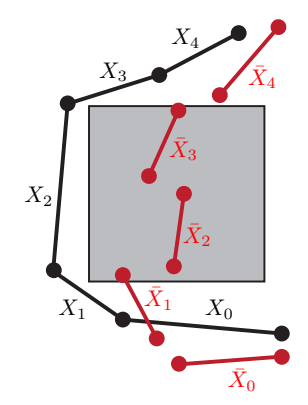


Fig. 3: ADMM maintain two sets of variables X_i and \bar{X}_i . Constraint satisfaction for X_i does not imply constraints satisfaction for \bar{X}_i .

A. Alternating Minimization (AM)

Before we describe our ADMM-type method, we review the basic alternating minimization scheme. AM has been used in trajectory optimization to handle time-optimality [36] and collision constraints [37]. A similar method can be applied to minimize Equation 5 that alternates between updating the separating plane n_i, d_i, n_{ij}, d_{ij} and the robot configurations θ as outlined in Algorithm 1. AM can be used along with ADMM while being easier to analyze. Prior work [37] did not provide a convergence analysis and Wang $et\ al.$ [36] setup the first order convergence for a specific, strictly convex objective function where each minimization subproblem is a single-valued map. In Section VII , we establish the convergence of Algorithm 1 for twice-differentiable objective functions with plane normals n_i, n_{ij} constrained to the unit-normal manifold.

In the next section, we will combine AM and ADMM, specifically we update robot configurations θ using ADMM and update separating planes n_i, d_i, n_{ij}, d_{ij} using AM.

B. ADMM with Stiffness Decoupling

The key idea behind ADMM is to treat stiff and non-stiff functions separately by introducing slack variables. Specifically, we introduce slack variables \bar{X}_i for each $i=1,\cdots,N$ and transforms Equation 5 into the following equivalent form:

By convention, we use a bar to indicate slack variables, i.e. $\bar{V}_i(s) = \dot{A}(s)\bar{X}_i$ and $\bar{A}_i(s) = \ddot{A}(s)\bar{X}_i$.

Remark 4.1: We choose to have all slack variables reside in Cartesian space. As a result, if non-linear forward kinematics functions are used, ADMM must handle nonlinear constraint $X_i(\theta) = \bar{X}_i$.

ADMM proceeds by transforming the equality constraints in Equation 6 into augmented Lagrangian terms. We arrive at the following augmented Lagrangian function:

$$\mathcal{L}(\theta, \Delta t, \Delta \bar{t}_i, \bar{X}_i, \lambda_i, n_i, d_i, n_{ij}, d_{ij}) \triangleq \sum_i \mathcal{O}(\bar{X}_i, \Delta \bar{t}_i) - \gamma \sum_i \log(v_{\text{max}} \Delta t - ||V_i||) - \gamma \sum_i \log(a_{\text{max}} \Delta t^2 - ||A_i||) - \gamma \sum_i \left[\sum_{x \in X_i} \log(n_i x(\theta) + d_i) + \sum_{z \in Z} \log(-n_i z - d_i) \right] - \gamma \sum_{ij} \left[\sum_{x \in X_i} \log(n_{ij} x(\theta) + d_{ij}) + \sum_{x \in X_j} \log(-n_{ij} x(\theta) - d_{ij}) \right] + \sum_i \frac{\varrho}{2} ||X_i(\theta) - \bar{X}_i||^2 + \lambda_i^T (X_i(\theta) - \bar{X}_i) + \sum_i \frac{\varrho}{2} ||\Delta t - \Delta \bar{t}_i||^2 + \Lambda_i^T (\Delta t - \Delta \bar{t}_i),$$

$$(7)$$

where ϱ is the penalty parameter, λ_i is the augmented Lagrangian multiplier for \bar{X}_i . We can now present our ADMM algorithm seeking stationary points of Equation 7. Each iteration of our Algorithm 2 is a five-way update that alternates between $\{\theta, \Delta t\}, \{\Delta \bar{t}_i, \bar{X}_i\}, \{\lambda_i, \Lambda_i\}, (n_i, d_i), (n_{ij}, d_{ij})$. Note that our objective function only appears in the $\{\Delta \bar{t}_i, \bar{X}_i\}$ -subproblem, which does not involve any stiff, log-barrier functions. Therefore, Algorithm 2 achieves stiffness decoupling.

Remark 4.2: For each optimization subproblem of Algorithm 2, we assume that the decision variable is initialized from last iteration. Our convergence proof does not require these optimization subproblems to be solved exactly. Instead, we only require a sufficient decrease condition for the objective function value or gradient norm (we refer readers to the appendices for more details).

Remark 4.3: ADMM always maintain two representations of the trajectory, X_i and \bar{X}_i , where X_i is used to satisfy the collision constraints and \bar{X}_i focuses on minimizing the

Algorithm 1: AM

```
Input: \theta^0, \Delta t^0, (n_i, d_i)^0, (n_{ij}, d_{ij})^0, assuming \mathcal{L} in Equation 5

1: for k = 0, 1, \cdots do

2: \theta^{k+1}, \Delta t^{k+1} \approx \underset{\theta, \Delta t}{\operatorname{argmin}} \mathcal{L}(\theta, \Delta t, n_i^k, d_i^k, n_{ij}^k, d_{ij}^k) \triangleright Update \theta, \Delta t

3: for collision-free constraint between ith piece of trajectory and environment do

4: (n_i, d_i)^{k+1} \approx \underset{\|n_i\|=1, d_i}{\operatorname{argmin}} \mathcal{L}(\theta^{k+1}, \Delta t^{k+1}, n_i, d_i, n_{ij}^k, d_{ij}^k)

5: for collision-free constraint between ith and jth piece of trajectory do

6: (n_{ij}, d_{ij})^{k+1} \approx \underset{\|n_{ij}\|=1, d_{ij}}{\operatorname{argmin}} \mathcal{L}(\theta^{k+1}, \Delta t^{k+1}, n_i^{k+1}, d_i^{k+1}, n_{ij}, d_{ij})
```

Algorithm 2: ADMM with Stiffness Decoupling

```
Input: \theta^0, \Delta t^0, \Delta \bar{t}_i^0, \bar{X}_i^0, \lambda_i^0, (n_i, d_i)^0, (n_{ij}, d_{ij})^0, assuming \mathcal{L} in Equation 7
  1: for k=0,1,\cdots do
2: \theta^{k+1}, \Delta t^{k+1} \approx \operatorname*{argmin} \mathcal{L}(\theta, \Delta t, \Delta \bar{t}_i, \bar{X}_i^k, \lambda_i^k, n_i^k, d_i^k, n_{ij}^k, d_{ij}^k)
                                                                                                                                                                                                                 \triangleright Update \theta, \Delta t, \bar{X}_i, \lambda_i
              3:
  4:
                    \lambda_{i}^{k+1} \leftarrow \lambda_{i}^{k} + \varrho(X_{i}(\theta^{k+1}) - \bar{X}_{i}^{k+1})
\Lambda_{i}^{k+1} \leftarrow \Lambda_{i}^{k} + \varrho(\Delta t^{k+1} - \Delta \bar{t}_{i}^{k+1})
  5:
  6:
              for collision-free constraint between ith piece of trajectory and environment do
  7:

    ○ Optimize separating plane

                    (n_i, d_i)^{k+1} \approx \operatorname{argmin} \mathcal{L}(\theta^{k+1}, \Delta t^{k+1}, \Delta \bar{t}_i^{k+1}, \bar{X}_i^{k+1}, \bar{\lambda}_i^{k+1}, n_i, d_i, n_{i,i}^k, d_{i,i}^k)
  8:
  9:
              for collision-free constraint between ith and jth piece of trajectory do
                    (n_{ij}, d_{ij})^{k+1} \approx \text{argmin } \mathcal{L}(\theta^{k+1}, \Delta t^{k+1}, \Delta \hat{t}_i^{k+1}, \bar{X}_i^{k+1}, \lambda_i^{k+1}, n_i^{k+1}, d_i^{k+1}, n_{ij}, d_{ij})
10:
```

objective function \mathcal{O} at the risk of violating the collision constraints, as illustrated in Figure 3. On convergence, the two representations coincide and both collision-free and local optimal conditions hold.

Remark 4.4: When updating the separating plane, the normal vector must be constrained to have unit length. These constraints can be reparameterized as an optimization on $\mathcal{SO}(3)$. Specifically, given the current solution denoted as n_{ij}^{curr} with $\|n_{ij}^{curr}\| = 1$, we reparameterize n_{ij} by premultiplying a rotation matrix $R = \exp(r)$ by n_{ij}^{curr} , where we use the Rodriguez formula to parameterize a rotation matrix as the exponential of an arbitrary 3-dimensional vector r. Instead of using n_{ij} as decision variables, we let $n_{ij} = \exp(r)n_{ij}^{curr}$ and use r as our decision variables. Whichever value r takes, we can ensure $\|n_{ij}\| = 1$ (we refer reads to [38] for more details).

V. EVALUATIONS

Our implementation uses C++11. Experiments are performed on a workstation with a 3.5 GHz Intel Core i9 processor. For experiments, we choose a unified set of parameters $v_{max} = 2m/s$, $a_{max} = 2m/s^2$ for UAVs (resp. $v_{max} = 0.1m/s$, $a_{max} = 0.1m/s^2$ for articulated bodies), $w = 10^8$, $\gamma = 10$, $\varrho = 0.1$ unless otherwise stated. We use a locally supported log-barrier function as done in our prior work [8], which is active only when the distance between two objects is less than 0.1m for UAVs (resp. 0.04m for articulated bodies). Further, we set our clearance distance to be 0.1m for UAVs (resp. $10^{-3}m$ for articulated bodies), which can be plugged into the continuous collision detector

used by our line-search algorithm. Our algorithm terminates when $\|\nabla_{\theta^{k+1}}\mathcal{L}\|_{\infty} < \epsilon$ and we choose $\epsilon = 10^{-2}$ for UAVs (resp. $\epsilon = 10^{-1}$ for articulated bodies). By comparing with our prior work [8], we demonstrate the ability of ADMM in terms of resolving stiff-coupling issues and boosting the overall perform. We further compare with prior works [39, 40] to highlight the robustness of our approach.

Fast Separating Plane Update: We found that iterative separating plane updates is a major computational bottleneck. Fortunately, mature collision detection algorithms such as the Gilbert–Johnson–Keerthi (GJK) algorithm [41] can quickly return the optimal separating direction. We emphasize that our separating planes minimizing the soft log-barrier penalties do not match the separating directions returned by GJK in general. However, we found that the separating plane return by GJK also leads to a reduction in the Lagrangian function, while being orders of magnitude faster to compute due to their highly optimized implementation. Therefore, we propose to use the GJK algorithm as long as the Lagrangian function is decreasing, which does not hinder our convergence guarantee.

Single-UAV Trajectory Planning: We first show six examples of trajectory optimization for a single UAV in complex environments as illustrated in Figure 4. For each example, we compare our method against two baselines [8, 40]. We initialize all three methods using the same feasible trajectory that is manually designed. Our AM Algorithm 1 takes from 133 to 93K(ms) to convergence and our ADMM Algorithm 2 takes 34 to 18.9K(ms). As compared with our prior work [8] that takes 1K to 420K(ms). In other words, we achieve from 22 to 82 times speedup over [8] while providing the

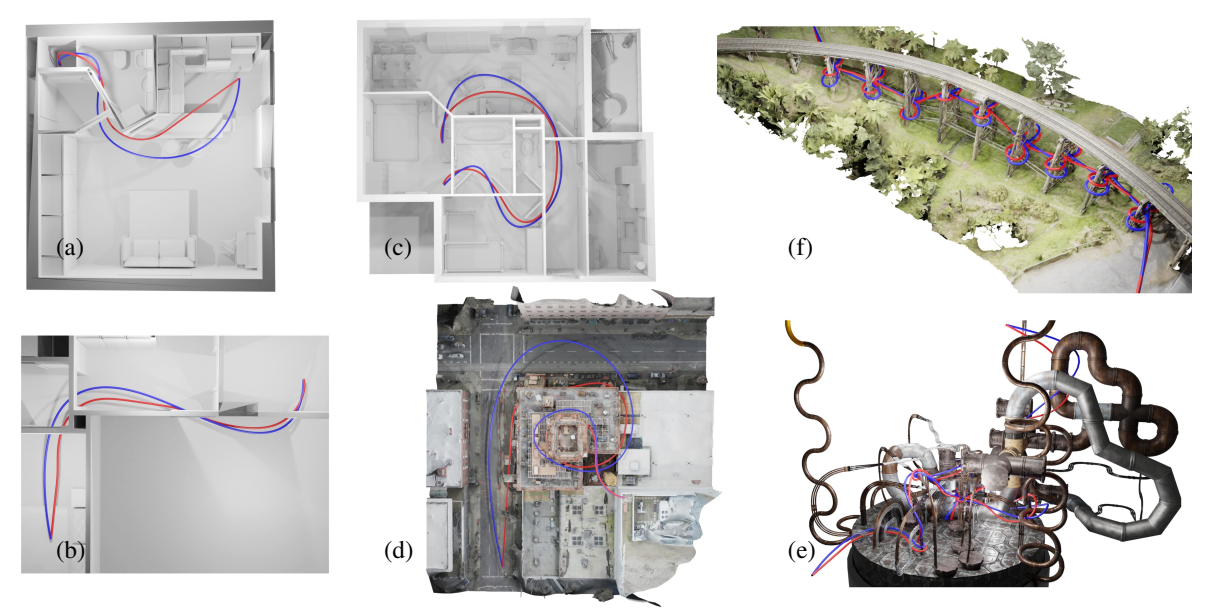


Fig. 4: Examples of a single UAV in complex environments: indoor flight (a-e) and bridge inspection (b).

	Trajectory Length (m) / Flying Time (s)							
	Example	Algorithm 1	Algorithm 2	[8]	[40]			
Ī	(a)	16.0/9.6	16.0/9.6	16.1/9.7	18.0/14.0			
	(b)	17.9/10.4	17.9/10.4	18.1/10.6	19.0/11.3			
	(c)	13.2/8.9	13.2/9.0	13.8/9.1	14.6/11.7			
	(d)	39.1/21.8	39.2/21.9	39.2/21.8	47.2/25.1			
	(e)	66.8/44.7	66.5/44.6	68.1/45.5	71.2/57.9			
	(f)	67.3/62.8	67.2/62.8	70.1/65.3	74.6/74.1			
Computational $Cost(ms)$								
ĺ	Example	Algorithm 1	Algorithm 2	[8]	[40]			
	(a)	388	45	1.0K	41			
	(b)	133	34	2.8K	50			
	(c)	313	123	7.8K	79			
	(d)	8.7K	938	34.3K	51			
	(e)	39.0K	6.4K	175.0K	864			
	(f)	92.9K	18.9K	420.1K	5.6K			
	(a) (b) (c) (d) (e)	Algorithm 1 388 133 313 8.7K 39.0K	Algorithm 2 45 34 123 938 6.4K	[8] 1.0K 2.8K 7.8K 34.3K 175.0K	41 50 79 51 864			

TABLE I: The quality of results in terms of trajectory length/flying time and computational cost of the three methods (ours, [8], and [40]) for the six examples of Figure 4.

trajectory of a similar quality. The convergence history of all three algorithms are summarized in Figure 5. Although the convergence speed is comparable in terms of number of iterations, our two methods (AM and ADMM) clearly outperform in terms of computational time. By not restricting the trajectory to precomputed corridors as done in [24, 42, 43, 40, 44], our method allows a larger solution space and returns a shorter trajectory. We summarize the quality of trajectory as computed by three methods in Table I.

Multi-UAV Trajectory Planning: We assume the trajectory of each UAV is represented by composite Bézier curves with degree M=5. Ideally, log-barrier functions should be added between every UAV-UAV and UAV-environment pair, incurring a quadratic cost. Instead, we use a bounding-volume hierarchy and only add collision-free constraints when the distance between two convex hulls are less than the activation distance of log-barrier function (0.1m). Note that this abrupt change in number of collision constraints will not hinder the convergence of ADMM because it can happen at most finitely many times. Our algorithm requires collision-free initial-guesses for all trajectories, and we compute these

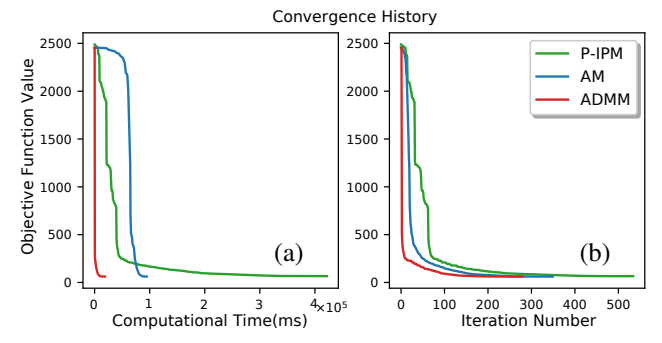


Fig. 5: Convergence history of various algorithms for the example in Figure 4 (f), comparing AM, ADMM, and Newton-type method (P-IPM) in terms of wall-time (a) and #Iterations (b).

initial trajectories using RRT connect. Our ADMM algorithm minimizes the jerk of each trajectory with time optimality as our objective function $O(\bar{X}_i, \Delta \bar{t}_i)$. Figure 6 shows two challenging problems. We further compare our method with [39], which uses soft penalty terms to push trajectories out of the obstacles. This work is complementary to our method, which allows initial guesses to penetrate obstacles but cannot ensure final result to be collision-free. Instead, our method must start from a collision-free initial guess and maintain the collision-free guarantee throughout the optimization. In Table II, we compare the quality of solutions and computational cost of these two methods.

Trajectory Length (m) / Flying Time (s) / Computational Co				
Example	Algorithm 2	[39]		
(a)	152.68/7.84/515	169.34/14.48/844.49		
(b)	71.33/14.57/2527	89.82/20.73/584.89		

TABLE II: The quality of results in terms of trajectory length/flying time and computational cost, comparing our method and [39].

Trajectory Planning for Articulated Robots: We highlight the performance of our method via an example involving two arms. We approximate each robot joint as a single convex object to reduce the number of separating planes. Our example is inspired by prior work [45], as illustrated in Figure 7, where

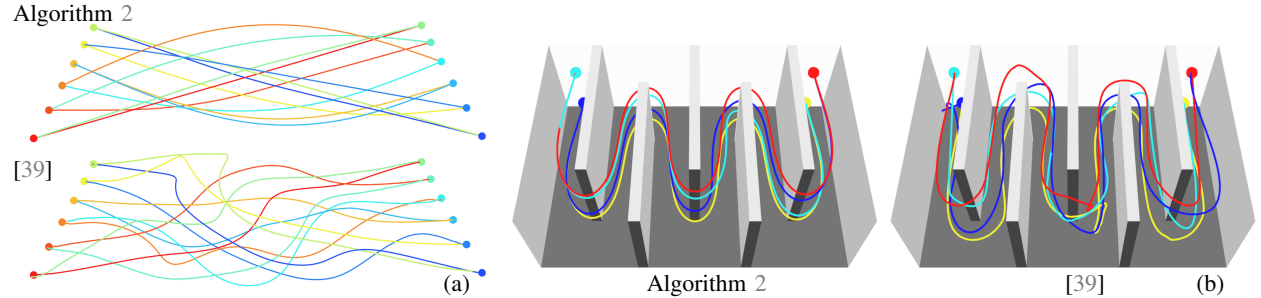


Fig. 6: Multiple UAV in complex environments, both with two groups of UAVs switching positions without (a) and with (b) obstacles.

we have two KUKA LWR robot arms (each with 8 joints) switch positions of their end-effectors. From RRT connect computed initial trajectory, our method can easily minimize acceleration of end-effects. The computational cost stiffness-decoupled ADMM is summarized in Table III and convergence history in Figure 8.

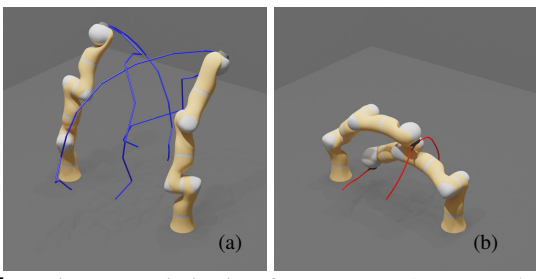


Fig. 7: Trajectory optimization for two KUKA LWR robot arms switching end-effector positions. (a): initial trajectory via RRT-connect; (b): optimized trajectory.

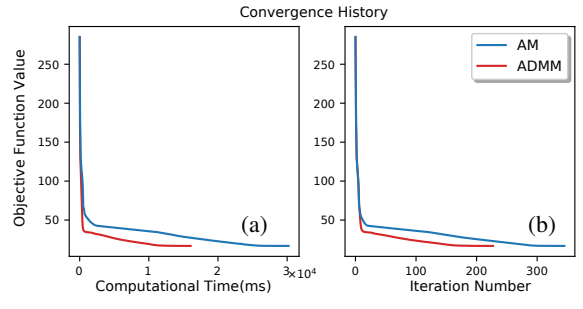


Fig. 8: Convergence history for the example in Figure 7, comparing AM and stiffness-decoupled ADMM in terms of wall-time (a) and #Iterations (b).

Trajectory Length (m) / Computational Cost (ms)						
RRT-connect	Algorithm 1	Algorithm 2				
6.38	1.63/30216	1.63/16118				

TABLE III: The quality of results in terms of trajectory length and computational cost, comparing our method and [46].

VI. CONCLUSION & LIMITATION

We propose a variant of ADMM-type solver for trajectory generation. We observe that the limited efficacy of our prior work [8] is mainly due to the stiff log-barrier functions corresponding to various hard constraints. Therefore, we propose to decompose stiff and non-stiff objective function terms using slack variables, while using additional constraints to ensure their consistency. ADMM originally applied this idea to convex optimizations and we establish its convergence guarantee under non-convex objectives and constraints that

arise from UAV and articulated robot trajectory planning problems. Our experiments confirm that ADMM successfully resolves stiff-coupling issues and achieves $10-100\times$ speedup over Newton-type algorithms. A major and common limitation of ADMM-type solvers is that convergence guarantee cannot be shown in more general scenarios, such as general control of nonlinear dynamic systems [28]. Although their empirical performances are promising, we lack theoretical explanations. In addition, the first-order convergence can have low-accuracy under insufficient iterations, where Anderson acceleration [47] can further boost the performance.

REFERENCES

- [1] C. Goerzen, Z. Kong, and B. Mettler, "A survey of motion planning algorithms from the perspective of autonomous uav guidance," *Journal of Intelligent and Robotic Systems*, vol. 57, no. 1, pp. 65–100, 2010.
- [2] T. Lee, M. Leok, and N. H. McClamroch, "Geometric tracking control of a quadrotor uav on se (3)," in 49th IEEE conference on decision and control (CDC), IEEE, 2010, pp. 5420–5425.
- [3] F. Augugliaro, A. P. Schoellig, and R. D'Andrea, "Generation of collision-free trajectories for a quadrocopter fleet: A sequential convex programming approach," in 2012 IEEE/RSJ international conference on Intelligent Robots and Systems, IEEE, 2012, pp. 1917–1922.
- [4] T. Kröger and F. M. Wahl, "Online trajectory generation: Basic concepts for instantaneous reactions to unforeseen events," *IEEE Transactions on Robotics*, vol. 26, no. 1, pp. 94–111, 2009.
- [5] K. Belghith, F. Kabanza, L. Hartman, and R. Nkambou, "Any-time dynamic path-planning with flexible probabilistic roadmaps," in *Proceedings 2006 IEEE International Conference on Robotics and Automation*, 2006. ICRA 2006., IEEE, 2006, pp. 2372–2377.
- [6] A. D. Ames, S. Coogan, M. Egerstedt, G. Notomista, K. Sreenath, and P. Tabuada, "Control barrier functions: Theory and applications," in 2019 18th European Control Conference (ECC), IEEE, 2019, pp. 3420–3431.
- [7] D. Panagou, "Motion planning and collision avoidance using navigation vector fields," in 2014 IEEE International Conference on Robotics and Automation (ICRA), IEEE, 2014, pp. 2513–2518.
- [8] R. Ni, T. Schneider, D. Panozzo, Z. Pan, and X. Gao, "Robust & asymptotically locally optimal uav-trajectory generation based on spline subdivision," arXiv:2010.09904, 2020.
- [9] L. F. Shampine and C. W. Gear, "A user's view of solving stiff ordinary differential equations," SIAM review, vol. 21, no. 1, pp. 1–17, 1979.
- [10] Y. Choi, M. Chen, Y. Choi, S. Briceno, and D. Mavris, "Multi-uav trajectory optimization utilizing a nurbs-based terrain model for an aerial imaging mission," *Journal of Intelligent & Robotic Systems*, vol. 97, no. 1, pp. 141–154, 2020.
- [11] M. Ragaglia, A. M. Zanchettin, and P. Rocco, "Trajectory generation algorithm for safe human-robot collaboration based on multiple depth sensor measurements," *Mechatronics*, vol. 55, pp. 267–281, 2018.
- [12] M. M. G. Ardakani, J. H. Cho, R. Johansson, and A. Robertsson, "Trajectory generation for assembly tasks via bilateral teleoperation," *IFAC Proceedings Volumes*, vol. 47, no. 3, pp. 10230–10235, 2014.
- [13] S. Shimoda, Y. Kuroda, and K. Iagnemma, "Potential field navigation of high speed unmanned ground vehicles on uneven terrain," in Proceedings of the 2005 IEEE International Conference on Robotics and Automation, IEEE, 2005, pp. 2828–2833.

- [14] Z. Qu, J. Wang, and C. E. Plaisted, "A new analytical solution to mobile robot trajectory generation in the presence of moving obstacles," *IEEE Transactions on Robotics*, vol. 20, no. 6, pp. 978–993, 2004.
- [15] M. Shomin and R. Hollis, "Differentially flat trajectory generation for a dynamically stable mobile robot," in 2013 IEEE International Conference on Robotics and Automation, IEEE, 2013, pp. 4467–4472.
- [16] S. Karaman, M. R. Walter, A. Perez, E. Frazzoli, and S. Teller, "Anytime motion planning using the rrt," in 2011 IEEE International Conference on Robotics and Automation, IEEE, 2011, pp. 1478–1483.
- [17] T. Ha and C.-H. Choi, "An effective trajectory generation method for bipedal walking," *Robotics and Autonomous Systems*, vol. 55, no. 10, pp. 795–810, 2007.
- [18] O. Von Stryk and R. Bulirsch, "Direct and indirect methods for trajectory optimization," *Annals of operations research*, vol. 37, no. 1, pp. 357–373, 1992.
- [19] J. T. Betts and W. P. Huffman, "Path-constrained trajectory optimization using sparse sequential quadratic programming," *Journal of Guidance, Control, and Dynamics*, vol. 16, no. 1, pp. 59–68, 1993.
- [20] E. Todorov, T. Erez, and Y. Tassa, "Mujoco: A physics engine for model-based control," in 2012 IEEE/RSJ International Conference on Intelligent Robots and Systems, IEEE, 2012, pp. 5026–5033.
- [21] F. Gao, Y. Lin, and S. Shen, "Gradient-based online safe trajectory generation for quadrotor flight in complex environments," in 2017 IEEE/RSJ International Conference on Intelligent Robots and Systems (IROS), 2017, pp. 3681–3688.
- [22] B. Zhou, F. Gao, L. Wang, C. Liu, and S. Shen, "Robust and efficient quadrotor trajectory generation for fast autonomous flight," *IEEE Robotics and Automation Letters*, vol. 4, no. 4, pp. 3529–3536, 2019.
- [23] X. Zhou, Z. Wang, H. Ye, C. Xu, and F. Gao, "Ego-planner: An esdf-free gradient-based local planner for quadrotors," *IEEE Robotics and Automation Letters*, vol. 6, no. 2, pp. 478–485, 2020.
- [24] S. Liu, M. Watterson, K. Mohta, K. Sun, S. Bhattacharya, C. J. Taylor, and V. Kumar, "Planning dynamically feasible trajectories for quadrotors using safe flight corridors in 3-d complex environments," *IEEE Robotics and Automation Letters*, vol. 2, no. 3, pp. 1688–1695, 2017.
- [25] J. Tordesillas and J. P. How, "FASTER: Fast and safe trajectory planner for navigation in unknown environments," *IEEE Transactions* on Robotics, 2021.
- [26] G. Vasudevan, L. T. Watson, and F. Lutze, "A homotopy approach for solving constrained optimization problems," in 1989 American Control Conference, IEEE, 1989, pp. 780–785.
- [27] S. Boyd, N. Parikh, and E. Chu, Distributed optimization and statistical learning via the alternating direction method of multipliers. Now Publishers Inc, 2011.
- [28] Z. Pan and D. Manocha, "Efficient solver for spacetime control of smoke," ACM Trans. Graph., vol. 36, no. 5, Jul. 2017.
- [29] Z. Cheng, J. Ma, X. Zhang, and T. H. Lee, "Semi-proximal admm for model predictive control problem with application to a uav system," in 2020 20th International Conference on Control, Automation and Systems (ICCAS), 2020, pp. 82–87.
- [30] Z. Zhou and Y. Zhao, "Accelerated admm based trajectory optimization for legged locomotion with coupled rigid body dynamics," in 2020 American Control Conference (ACC), IEEE, 2020, pp. 5082–5089.
- [31] B. Jiang, T. Lin, S. Ma, and S. Zhang, "Structured nonconvex and nonsmooth optimization: Algorithms and iteration complexity analysis," *Computational Optimization and Applications*, vol. 72, no. 1, pp. 115–157, 2019.
- [32] Y. Wang, W. Yin, and J. Zeng, "Global convergence of admm in nonconvex nonsmooth optimization," *Journal of Scientific Computing*, vol. 78, no. 1, pp. 29–63, 2019.
- [33] W. Gao, D. Goldfarb, and F. E. Curtis, "Admm for multiaffine constrained optimization," *Optimization Methods and Software*, vol. 35, no. 2, pp. 257–303, 2020.
- [34] C. Katrakazas, M. Quddus, W.-H. Chen, and L. Deka, "Real-time motion planning methods for autonomous on-road driving: State-ofthe-art and future research directions," *Transportation Research Part* C: Emerging Technologies, vol. 60, pp. 416–442, 2015
- C: Emerging Technologies, vol. 60, pp. 416–442, 2015.
 [35] P. Cheng, J. Keller, and V. Kumar, "Time-optimal uav trajectory planning for 3d urban structure coverage," in 2008 IEEE/RSJ International Conference on Intelligent Robots and Systems, IEEE, 2008, pp. 2750–2757.
- [36] Z. Wang, X. Zhou, C. Xu, J. Chu, and F. Gao, "Alternating minimization based trajectory generation for quadrotor aggressive flight," *IEEE RA-L*, vol. 5, no. 3, pp. 4836–4843, 2020.

- [37] W. Hönig, J. A. Preiss, T. K. S. Kumar, G. S. Sukhatme, and N. Ayanian, "Trajectory planning for quadrotor swarms," *IEEE Transactions on Robotics*, vol. 34, no. 4, pp. 856–869, 2018.
- [38] C. J. Taylor and D. J. Kriegman, "Minimization on the lie group so (3) and related manifolds," 1994.
- [39] X. Zhou, X. Wen, J. Zhu, H. Zhou, C. Xu, and F. Gao, "Ego-swarm: A fully autonomous and decentralized quadrotor swarm system in cluttered environments," arXiv:2011.04183, 2020.
- [40] Z. Han, Z. Wang, N. Pan, Y. Lin, C. Xu, and F. Gao, "Fast-racing: An open-source strong baseline for se (3) planning in autonomous drone racing," *IEEE Robotics and Automation Letters*, 2021.
- [41] M. Montanari, N. Petrinic, and E. Barbieri, "Improving the gjk algorithm for faster and more reliable distance queries between convex objects," ACM Transactions on Graphics (TOG), vol. 36, no. 3, pp. 1–17, 2017.
- [42] F. Gao, W. Wu, Y. Lin, and S. Shen, "Online safe trajectory generation for quadrotors using fast marching method and bernstein basis polynomial," in 2018 IEEE International Conference on Robotics and Automation (ICRA), 2018, pp. 344–351.
- [43] J. Tordesillas, B. T. Lopez, and J. P. How, "FASTER: Fast and safe trajectory planner for flights in unknown environments," in 2019 IEEE/RSJ International Conference on Intelligent Robots and Systems (IROS), IEEE, 2019.
- [44] Z. Wang, X. Zhou, C. Xu, and F. Gao, "Geometrically constrained trajectory optimization for multicopters," arXiv:2103.00190, 2021.
- [45] H. Ha, J. Xu, and S. Song, "Learning a decentralized multi-arm motion planner," in Conference on Robotic Learning (CoRL), 2020.
- [46] K. Hauser, "Semi-infinite programming for trajectory optimization with non-convex obstacles," *The International Journal of Robotics Research*, vol. 40, no. 10-11, pp. 1106–1122, 2021.
- [47] J. Zhang, B. O'Donoghue, and S. Boyd, "Globally convergent typei anderson acceleration for nonsmooth fixed-point iterations," SIAM Journal on Optimization, vol. 30, no. 4, pp. 3170–3197, 2020.
- [48] Y. Xu and W. Yin, "A globally convergent algorithm for nonconvex optimization based on block coordinate update," *Journal of Scientific Computing*, vol. 72, no. 2, pp. 700–734, 2017.
- [49] Q. Deng and C. Lan, "Efficiency of coordinate descent methods for structured nonconvex optimization," arXiv:1909.00918, 2019.
- [50] W. Ring and B. Wirth, "Optimization methods on riemannian manifolds and their application to shape space," SIAM Journal on Optimization, vol. 22, no. 2, pp. 596–627, 2012.
- [51] S. Lojasiewicz, "A topological property of real analytic subsets," Coll. du CNRS, Les équations aux dérivées partielles, pp. 87–89, 1963.

VII. CONVERGENCE ANALYSIS: ALTERNATING MINIMIZATION (AM)

Throughout our analysis, we assume the objective function O is twice-differentiable. We rewrite the Lagrangian Equation 5 as a function in the three (sets of) variables, Θ, P_i, P_{ij} , where we define the shorthand notation $\Theta \triangleq (\theta, \Delta t), P_i \triangleq$ (n_i, d_i) , and $P_{ij} \triangleq (n_{ij}, d_{ij})$. We also denote $P \triangleq (n, d)$ as an arbitrary plane, which can be some P_i or P_{ij} . During the kth iteration, these three variables will be updated in order and Algorithm 1 will generate an infinite sequence $\{(\Theta^k, P_i^k, P_{ij}^k)\}$. We further assume that each minimization subproblem of Algorithm 1, e.g., the Θ^k -subproblem, is warmstarted from its previous value Θ^{k-1} . The convergence of AM in non-convex settings has been shown in prior work [48], but they assume the log-barrier functions are proximable, which does not hold in our case due to the non-linear forward kinematics $x(\theta)$. Other work such as [49] assumes the availability of a global Lipschitz constant, which does not hold for a log-barrier function. We overcome this difficulty by using a line-search to ensure the satisfaction of Armijo's condition for solving the three subproblems. In other words, Line 2 of Algorithm 1 is implemented in Algorithm 3. To implement Line 4 and Line 6 of Algorithm 1, we handle the additional unit-norm constraint on n_i and n_{ij} via Riemannian optimization [50]. Taking an arbitrary P for example, we start from a feasible initial guess ||n|| = 1 and optimize on the tangent space $v \in \mathcal{T}_n S^2$. The optimized v provides an updated $P = (\exp_n v, d)$. Essentially, we use standard line-search as outlined in Algorithm 4 to optimize the function $\mathcal{L}(\exp_n v, d)$ denoted as $\mathcal{L} \circ \exp_n$. We further use a shorthand notation $\mathcal{L} \circ \exp(\theta, \Delta t, v_i, d_i, v_{ij}, d_{ij})$ to denote the reparameterization of \mathcal{L} with each n_i (w.r.t. n_{ij}) replaced by $\exp_{n_i}(v_i)$ (w.r.t. $\exp_{n_{ij}}(v_{ij})$). A direct verification shows that a first-order critical point of \mathcal{L} is a point with $\|\nabla \mathcal{L} \circ \exp\| = 0$.

Algorithm 3: Line-Search Gradient Descent

```
Input: Initial guess \Theta, c \in (0,1), \gamma \in (0,1)

1: \alpha \leftarrow 1

2: while \mathcal{L}(\Theta - \alpha \nabla_{\Theta} \mathcal{L}(\Theta)) > \mathcal{L}(\Theta) - c\alpha \|\nabla_{\Theta} \mathcal{L}(\Theta)\|^2 do

3: \alpha \leftarrow \gamma \alpha

4: Return \Theta - \alpha \nabla_{\Theta} \mathcal{L}(\Theta)
```

Algorithm 4: Riemannian Line-Search Gradient Descent

To establish convergence to first-order critical point, we bound the magnitude of α making use of the Lipschitz constant of a function. In the following analysis, we omit some parameters of $\mathcal L$ for brevity, where the omitted parameters is same as Algorithm 1.

Lemma 7.1: Consider a function $\mathcal{L}(\Theta)$. Assume that $\nabla_{\Theta}\mathcal{L}(\Theta)$ is L-Lipschitz continuous within some convex set

B. If Algorithm 3 updates Θ^k to Θ^{k+1} with $\Theta^k, \Theta^{k+1} \in B$, then we have: $\alpha \geq 2\gamma(1-c)/L$ and $\mathcal{L}(\Theta^{k+1}) + c\|\Theta^{k+1} - \Theta^k\|^2 \leq \mathcal{L}(\Theta^k)$.

Proof: When $\alpha \le 2(1-c)/L$, we have:

$$\begin{split} \mathcal{L}(\boldsymbol{\Theta}^{k+1}) \leq & \mathcal{L}(\boldsymbol{\Theta}^{k}) + \langle \nabla_{\boldsymbol{\Theta}} \mathcal{L}(\boldsymbol{\Theta}^{k}), \boldsymbol{\Theta}^{k+1} - \boldsymbol{\Theta}^{k} \rangle + \frac{L}{2} \|\boldsymbol{\Theta}^{k+1} - \boldsymbol{\Theta}^{k}\|^{2} \\ = & \mathcal{L}(\boldsymbol{\Theta}^{k}) + (\frac{L\alpha^{2}}{2} - \alpha) \|\nabla_{\boldsymbol{\Theta}} \mathcal{L}(\boldsymbol{\Theta}^{k})\|^{2} \\ \leq & \mathcal{L}(\boldsymbol{\Theta}^{k}) - c\alpha \|\nabla_{\boldsymbol{\Theta}} \mathcal{L}(\boldsymbol{\Theta}^{k})\|^{2}. \end{split}$$

By the logic of Algorithm 3, we have the first inequality:

$$\alpha \ge \gamma^{\lceil \log_{\gamma}(2(1-c)/L) \rceil} \ge 2\gamma(1-c)/L.$$
 (8)

The second inequality follows from the Armijo's condition:

$$\mathcal{L}(\Theta^{k+1}) + c \|\Theta^{k+1} - \Theta^k\|^2 = \mathcal{L}(\Theta^{k+1}) + c\alpha^2 \|\nabla_{\Theta}\mathcal{L}(\Theta^k)\|^2$$

$$\leq \mathcal{L}(\Theta^k) - c\alpha \|\nabla_{\Theta}\mathcal{L}(\Theta^k)\|^2 + c\alpha^2 \|\nabla_{\Theta}\mathcal{L}(\Theta^k)\|^2 \leq \mathcal{L}(\Theta^k), \quad (9)$$

where we have used $\alpha \leq 1$.

Given the above results, it is straightforward to establish the convergence guarantee for a convergent sub-sequence.

Lemma 7.2: If \mathcal{L} is lower-bounded, then every accumulation point of the sequence $\{(\Theta^k, P_i^k, P_{ij}^k)\}$ generated by Algorithm 1 is a critical point. Suppose the sequence is convergent, the local convergence speed of $\|\nabla \mathcal{L} \circ \exp\|$ is $\mathcal{O}(1/\sqrt{K})$.

Proof: The function $\{\mathcal{L}(\Theta^k, P_i^k, P_{ij}^k)\}$ is monotonically decreasing and bounded from below, so it converges to $\mathcal{L}(\bar{\Theta}, \bar{P}_i, \bar{P}_{ij})$ by continuity, where $(\bar{\Theta}, \bar{P}_i, \bar{P}_{ij})$ is an accumulation point with the convergent sub-sequence identified by the index subset: $\mathcal{K} \subset \{k | k = 1, 2, \cdots\}$.

Applying Lemma 7.1: Invoke Equation 9 for \mathcal{L} in Algorithm 3 and we will have:

$$\mathcal{L}(\Theta^{k+1}) + c \|\Theta^{k+1} - \Theta^k\|^2 \le \mathcal{L}(\Theta^k).$$

Invoke Equation 9 for $\mathcal{L} \circ \exp_n$ in Algorithm 4 and we will have:

$$\mathcal{L}(P^{k+1}) + c||v^k||^2 + c||d^{k+1} - d^k||^2 \le \mathcal{L}(P^k).$$

Summing up the above equations for all the iterations of Algorithm 1 and we have:

$$\sum_{k=0}^{\infty} \|\Theta^{k+1} - \Theta^{k}\|^{2} + \sum_{k=0}^{\infty} \sum_{i} \|(v_{i}^{k}, d_{i}^{k+1}) - (0, d_{i}^{k})\|^{2} + \sum_{k=0}^{\infty} \sum_{ij} \|(v_{ij}^{k}, d_{ij}^{k+1}) - (0, d_{ij}^{k})\|^{2} \le \frac{\mathcal{L}(\Theta^{0}, P_{i}^{0}, P_{ij}^{0}) - \mathcal{L}(\bar{\Theta}, \bar{P}_{i}, \bar{P}_{ij})}{c} < \infty.$$

We conclude that $\lim_{k\to\infty} \|\Theta^{k+1} - \Theta^k\| = 0$, $\lim_{k\to\infty} \|v^k\| = 0$, and $\lim_{k\to\infty} \|d^{k+1} - d^k\| = 0$ for any P. Here we use shorthand notation v_i^k (w.r.t. v_{ij}^k) to denote v found by Algorithm 4 for P_i (w.r.t. P_{ij}).

Optimality & Convergence Speed of Θ : $\operatorname{dom} \mathcal{L}$ is dictated by the log-barrier function, which is an open set. $\mathcal{L}(\bar{\Theta}, \bar{P}_i, \bar{P}_{ij}) < \infty$ so that $(\bar{\Theta}, \bar{P}_i, \bar{P}_{ij})$ is within the open set. As a result, we can find some small neighborhood $B_{\rho}(\bar{\Theta}, \bar{P}_i, \bar{P}_{ij}) \subset \operatorname{dom} \mathcal{L}$ (denoted as B_{ρ} for short) such that $(\Theta^k, P_i^k, P_{ij}^k) \in B_{\rho/2}$ and $\|\Theta^{k+1} - \Theta^k\| \le \rho/2$ for any sufficiently large $\mathcal{K} \ni k > k_0$, where ρ is some small positive number. W.l.o.g., we can discard the sequence before k_0 and

assume $k_0=0$. We can choose a sufficiently small ρ such that $\nabla_{\Theta}\mathcal{L}$ is L-Lipschitz continuous within $B_{\rho}\subset \mathrm{dom}\mathcal{L}$. Invoke Equation 8 for \mathcal{L} in Algorithm 3 and we will have:

$$\begin{split} 0 &= \lim_{\mathcal{K}\ni k\to\infty} \|\boldsymbol{\Theta}^{k+1} - \boldsymbol{\Theta}^k\| = \lim_{\mathcal{K}\ni k\to\infty} \alpha^k \|\nabla_{\boldsymbol{\Theta}} \mathcal{L}(\boldsymbol{\Theta}^k)\| \\ &\geq 2\gamma (1-c)/L \lim_{\mathcal{K}\ni k\to\infty} \|\nabla_{\boldsymbol{\Theta}} \mathcal{L}(\boldsymbol{\Theta}^k)\| = 2\gamma (1-c)/L \|\nabla_{\boldsymbol{\Theta}} \mathcal{L}(\bar{\boldsymbol{\Theta}})\|, \end{split}$$

where α^k is the α used in the line-search during the k-th iteration. If the entire sequence is convergent, then we have the following result for the local convergence speed:

$$K(2\gamma(1-c)/L)^{2} \min_{k=0,\dots,K} \|\nabla_{\Theta} \mathcal{L}(\Theta^{k})\|^{2}$$

$$\leq (2\gamma(1-c)/L)^{2} \sum_{k=0}^{K} \|\nabla_{\Theta} \mathcal{L}(\Theta^{k})\|^{2} \leq \sum_{k=0}^{K} \|\Theta^{k+1} - \Theta^{k}\|^{2}$$

$$\leq \sum_{k=0}^{\infty} \|\Theta^{k+1} - \Theta^{k}\|^{2} < \infty.$$

Optimality & Convergence Speed of \bar{P} : We can also choose sufficiently small ρ such that for any fixed $(\Theta^k, P_i^k, P_{ij}^k) \in B_\rho \subset \text{dom}\mathcal{L}$, the function $\nabla_{v,d}\mathcal{L} \circ \exp_n$ is L-Lipschitz continuous within B_ρ . We invoke Equation 8 for $\mathcal{L} \circ \exp$ in Algorithm 3 and following the same logic as that of $\bar{\Theta}$.

Note that we cannot have overall convergence speed due to a lack of a global Lipschitz constant. To get rid of the whole sequence convergence assumption and establish a local convergence speed and the convergence of entire sequence $\{(\Theta^k, P_i^k, P_{ij}^k)\}$, we need the KŁ property [51] of \mathcal{L} , which is a rather mild assumption that holds for all real analytic functions. Specifically, we assume the KŁ property [51] holds for the composite function $\mathcal{L} \circ \exp$ defined below:

Definition 7.3: The function $\mathcal{L} \circ \exp$ satisfies the KŁ property at some point $(\bar{\Theta}, \bar{P}_i, \bar{P}_{ij})$, if there exists a neighborhood B_{ρ} and a convex function ϕ such that, for any $(\Theta, \bar{P}_i, \bar{P}_{ij}) \in B_{\rho}$, we have:

$$\phi'(\mathcal{L}(\Theta, P_i, P_{ij}) - \mathcal{L}(\bar{\Theta}, \bar{P}_i, \bar{P}_{ij}))$$

$$\|\nabla \mathcal{L}(\Theta, \exp_{n_i}(0), d_i, \exp_{n_{ij}}(0), d_{ij})\| \ge 1.$$

We establish the convergence of sequence $\{(\Theta^k, P_i^k, P_{ij}^k)\}$ and the local convergence speed assuming the KŁ property.

Lemma 7.4: If $\mathcal{L} \circ \exp$ is lower-bounded and pertains the KŁ property (Definition 7.3), and the sequence $\{(\Theta^k, P_i^k, P_{ij}^k)\}$ generated by Algorithm 1 has a finite accumulation point, then the sequence is convergent.

Proof: We denote (Θ, P_i, P_{ij}) as the accumulation point. By invoking Lemma 7.2, we know that $\nabla \mathcal{L} \circ \exp = 0$. W.l.o.g., we assume $\mathcal{L}(\bar{\Theta}, \bar{P}_i, \bar{P}_{ij}) = 0$. By continuity, we can choose a small neighborhood $B_{2\rho} \subset \text{dom}\mathcal{L}$ where $\|\nabla \mathcal{L} \circ \exp\| < \epsilon$ and the the KŁ property holds. We further denote $\nabla \mathcal{L} \circ \exp$ as L-Lipschitz continuous within $B_{2\rho}$. Finally, in a sufficiently small local neighborhood, we can setup strong equivalence between metrics in tangent space and ambient space. In other words, we can find two positive constants \underline{L} and \bar{L} such that:

$$\underline{L}\|\exp_n v - \exp_n v'\| \le \|v - v'\| \le \bar{L}\|\exp_n v - \exp_n v'\|,$$

for any point in $B_{2\rho}$. If we start from $\left(\Theta^k, P_i^k, P_{ij}^k\right) \in B_{\rho}$, we choose sufficiently large k_0 such that the subsequent point $\left(\Theta^{k+1}, P_i^{k+1}, P_{ij}^{k+1}\right) \in B_{2\rho}$ for every $k \geq k_0$ due to

Lemma 7.2. W.l.o.g., we can assume $k_0 = 0$. Let's now define two constants:

$$L_1 \triangleq \max\left(\frac{L}{2\gamma(1-c)} + \sum_i L + \sum_{ij} L, \frac{L\bar{L}}{2\gamma(1-c)}\right)$$

$$L_2 \triangleq \min(c, cL^2).$$

Since there is a sub-sequence converging to $(\bar{\Theta}, \bar{P}_i, \bar{P}_{ij})$, we can choose large enough $k \ge k_0$ such that:

$$\|\left(\Theta^k, P_i^k, P_{ij}^k\right) - \left(\bar{\Theta}, \bar{P}_i, \bar{P}_{ij}\right)\| \le \rho - L_1/L_2\phi(\mathcal{L}\left(\Theta^k, P_i^k, P_{ij}^k\right)).$$

W.l.o.g., we can assume $k_0 = 0$ and:

$$(\Theta^{0}, P_{i}^{0}, P_{ij}^{0}) \in B_{\rho - L_{1}/L_{2}\phi(\mathcal{L}(\Theta^{0}, P_{i}^{0}, P_{ij}^{0}))}.$$
(10)

Next, we show that every $\left(\Theta^k,P_i^k,P_{ij}^k\right)\in B_\rho$ by induction. If we already have $\left(\Theta^0,P_i^0,P_{ij}^0\right),\cdots,\left(\Theta^k,P_i^k,P_{ij}^k\right)\in B_\rho$, then the following holds for $\left(\Theta^{k+1},P_i^{k+1},P_{ij}^{k+1}\right)\in B_\rho$:

$$\frac{\mathcal{L}\left(\Theta^{k}, P_{i}^{k}, P_{ij}^{k}\right) - \mathcal{L}\left(\Theta^{k+1}, P_{i}^{k+1}, P_{ij}^{k+1}\right)}{\phi(\mathcal{L}\left(\Theta^{k}, P_{i}^{k}, P_{ij}^{k}\right)) - \phi(\mathcal{L}\left(\Theta^{k+1}, P_{i}^{k+1}, P_{ij}^{k+1}\right))} \\
\leq 1/\phi'(\mathcal{L}\left(\Theta^{k}, P_{i}^{k}, P_{ij}^{k}\right)) \\
\leq \|\nabla \mathcal{L}(\Theta^{k}, \exp_{n_{i}^{k}}(0), d_{i}^{k}, \exp_{n_{ij}^{k}}(0), d_{ij}^{k})\| \\
= \|\nabla \Theta \mathcal{L}(\Theta^{k})\| + \sum_{i} \|\nabla_{v,d}\mathcal{L} \circ \exp_{n_{i}^{k}}(0, d_{i}^{k})\| + \sum_{ij} \|\nabla_{v,d}\mathcal{L} \circ \exp_{n_{ij}^{k}}(0, d_{ij}^{k}))\| \\
\leq \frac{\|\Theta^{k+1} - \Theta^{k}\|}{\alpha_{\Theta}^{k}} + \sum_{i} \left[\frac{\|\left(v_{i}^{k}, d_{i}^{k+1} - d_{i}^{k}\right)\|}{\alpha_{n_{i,d_{i}}}^{k}} + \mathcal{L}\|\Theta^{k+1} - \Theta^{k}\| \right] + \sum_{ij} \left[\frac{\|\left(v_{ij}^{k}, d_{ij}^{k+1} - d_{ij}^{k}\right)\|}{\alpha_{n_{ij},d_{ij}}^{k}} + \mathcal{L}\|\Theta^{k+1} - \Theta^{k}\| \right] \\
\leq \left[\frac{\mathcal{L}}{2\gamma(1-c)} + \sum_{i} \mathcal{L} + \sum_{ij} \mathcal{L} \right] \|\Theta^{k+1} - \Theta^{k}\| + \sum_{ij} \|\left(v_{ij}^{k}, d_{ij}^{k+1} - d_{ij}^{k}\right)\| + \sum_{ij} \|\left(v_{ij}^{k}, d_{ij}^{k+1} - d_{ij}^{k}\right)\| \right] \\
\leq \left[\frac{\mathcal{L}}{2\gamma(1-c)} + \sum_{i} \mathcal{L} + \sum_{ij} \mathcal{L} \right] \|\Theta^{k+1} - \Theta^{k}\| + \sum_{ij} \|\mathcal{L}_{ij} - \mathcal{L}_{ij} - \mathcal{L}_{ij} - \mathcal{L}_{ij} \right] \\
\leq \mathcal{L}_{ij} \left[\sum_{i} \|P_{i}^{k+1} - P_{i}^{k}\| + \sum_{ij} \|P_{ij}^{k+1} - P_{ij}^{k}\| \right] \\
\leq \mathcal{L}_{1} \|\left(\Theta^{k+1}, P_{i}^{k+1}, P_{ij}^{k+1}\right) - \left(\Theta^{k}, P_{i}^{k}, P_{ij}^{k}\right) \|, \tag{11}$$

where we use shorthand notation α_{Θ}^k (w.r.t. $\alpha_{n_i,d_i}^k, \alpha_{n_{ij},d_{ij}}^k$) to denote α found by Algorithm 3 for Θ (w.r.t. P_i, P_{ij}). The first inequality above is due to the convexity of ϕ . The second inequality is due to the KŁ property of $\mathcal{L} \circ \exp$. The third inequality is due to the logic of line-search algorithms and L-Lipschitz continuity of gradient within $B_{2\rho}$. The forth inequality is due to Lemma 7.2 and the fifth inequality is due to the strong metric equivalently, both within $B_{2\rho}$. We further have the following estimate of function decrease due to Lemma 7.2:

$$\begin{split} &\mathcal{L}\left(\Theta^{k}, P_{i}^{k}, P_{ij}^{k}\right) - \mathcal{L}\left(\Theta^{k+1}, P_{i}^{k+1}, P_{ij}^{k+1}\right) \\ & \geq c\|\Theta^{k+1} - \Theta^{k}\|^{2} + c\sum_{i}\|v_{i}^{k}\|^{2} + c\sum_{i}\|d_{i}^{k+1} - d_{i}^{k}\|^{2} + \\ & c\sum_{ij}\|v_{ij}^{k}\|^{2} + c\sum_{ij}\|d_{ij}^{k+1} - d_{ij}^{k}\|^{2} \\ & \geq c\|\Theta^{k+1} - \Theta^{k}\|^{2} + c\underline{L}^{2}\sum_{i}\|n_{i}^{k+1} - n_{i}^{k}\|^{2} + c\sum_{i}\|d_{i}^{k+1} - d_{i}^{k}\|^{2} + c\sum_{i}\|d_{i}^{k}\|^{2} + c\sum_{i}\|d_{i}\|^{2$$

$$c\underline{L}^{2} \sum_{ij} \|n_{ij}^{k+1} - n_{ij}^{k}\|^{2} + c \sum_{ij} \|d_{ij}^{k+1} - d_{ij}^{k}\|^{2}$$

$$\geq L_{2} \|\left(\Theta^{k+1}, P_{i}^{k+1}, P_{ij}^{k+1}\right) - \left(\Theta^{k}, P_{i}^{k}, P_{ij}^{k}\right)\|^{2}. \tag{12}$$

Combining Equation 11 and Equation 12, we conclude that:

$$\phi(\mathcal{L}(\Theta^{k}, P_{i}^{k}, P_{ij}^{k})) - \phi(\mathcal{L}(\Theta^{k+1}, P_{i}^{k+1}, P_{ij}^{k+1}))
\ge L_{2}/L_{1} \|(\Theta^{k+1}, P_{i}^{k+1}, P_{ij}^{k+1}) - (\Theta^{k}, P_{i}^{k}, P_{ij}^{k})\|.$$
(13)

The above property holds for all $0, \dots, k$ so we can sum these equations up to derive:

$$\begin{split} & \| \left(\Theta^{k+1}, P_i^{k+1}, P_{ij}^{k+1} \right) - \left(\bar{\Theta}, \bar{P}_i, \bar{P}_{ij} \right) \| \\ = & \| \left(\bar{\Theta}, \bar{P}_i, \bar{P}_{ij} \right) - \left(\Theta^0, P_i^0, P_{ij}^0 \right) \| + \\ & \| \left(\Theta^{k+1}, P_i^{k+1}, P_{ij}^{k+1} \right) - \left(\Theta^0, P_i^0, P_{ij}^0 \right) \| \\ \leq & \| \left(\bar{\Theta}, \bar{P}_i, \bar{P}_{ij} \right) - \left(\Theta^0, P_i^0, P_{ij}^0 \right) \| + \\ & L_1 / L_2 \left[\phi (\mathcal{L} \left(\Theta^0, P_i^0, P_{ij}^0 \right) \right) - \phi (\mathcal{L} \left(\Theta^{k+1}, P_i^{k+1}, P_{ij}^{k+1} \right) \right) \right] \\ \leq & \rho - L_1 / L_2 \phi (\mathcal{L} \left(\Theta^0, P_i^0, P_{ij}^0 \right) \right) + \\ & L_1 / L_2 \left[\phi (\mathcal{L} \left(\Theta^0, P_i^0, P_{ij}^0 \right) \right) - \phi (\mathcal{L} \left(\Theta^{k+1}, P_i^{k+1}, P_{ij}^{k+1} \right) \right) \right] \leq \rho, \end{split}$$

where we have used Equation 10 in the second to last inequality. By induction, we conclude that every element of $(\Theta^k, P_i^k, P_{ij}^k) \in B_\rho$ and we have from Equation 13:

$$\sum_{k=0}^{\infty} \| \left(\Theta^{k+1}, P_i^{k+1}, P_{ij}^{k+1} \right) - \left(\Theta^k, P_i^k, P_{ij}^k \right) \| < \infty,$$

which shows that the sequence $\{(\Theta^k, P_i^k, P_{ij}^k)\}$ is a Cauchy sequence and is thus convergent. Since $(\bar{\Theta}, \bar{P}_i, \bar{P}_{ij})$ is a limit point of the sequence, we conclude that the entire sequence converge to $(\bar{\Theta}, \bar{P}_i, \bar{P}_{ij})$ with local convergence speed being $\mathcal{O}(1/\sqrt{K})$ due to Lemma 7.2.

VIII. CONVERGENCE ANALYSIS: ADMM WITH STIFFNESS DECOUPLING

We prove the convergence of Algorithm 2 which is similar to [31] but we deviate from their prove in that 1) we consider nonlinear constraints and 2) we consider a Lagrangian function (Equation 7) that is not Lipschitz continuous. To simplify notation, we present our proof without variable Δt and Δt , i.e., we assume $\Theta = \theta$ in the following proof. In fact, the identical proof can be extended to the case with time-optimality. Specifically, if we adopt the following change of variable, the case with time optimality is proved:

$$\theta \leftarrow \begin{pmatrix} \theta \\ \Delta t \end{pmatrix} \quad X_i(\theta) \leftarrow \begin{pmatrix} X_i(\theta) \\ \Delta t \end{pmatrix} \quad \bar{X}_i \leftarrow \begin{pmatrix} \bar{X}_i \\ \Delta \bar{t}_i \end{pmatrix} \quad \lambda_i \leftarrow \begin{pmatrix} \lambda_i \\ \Lambda_i \end{pmatrix}.$$

We take the same assumptions on \mathcal{O} as that of Section VII. The only different from Algorithm 1 lies in Line 4 and Line 5 of Algorithm 2. First, it is not practical to solve the \bar{X}_i^{k+1} -subproblem exactly and we adopt the linear proximal operator instead:

$$\bar{X}_{i}^{k+1} = \underset{\bar{X}_{i}}{\operatorname{argmin}} \frac{\beta}{2} \| \bar{X}_{i} - \bar{X}_{i}^{k} \| + \\
\langle \nabla_{\bar{X}_{i}} \mathcal{L}(\theta^{k+1}, \bar{X}_{i}, \lambda_{i}^{k}, n_{i}^{k}, d_{i}^{k}, n_{ij}^{k}, d_{ij}^{k}), \bar{X}_{i} - \bar{X}_{i}^{k} \rangle \\
= \bar{X}_{i}^{k} - \frac{1}{\beta} \left[\nabla \mathcal{O}(\bar{X}_{i}^{k}) + \varrho(\bar{X}_{i}^{k} - X_{i}(\theta^{k+1})) - \lambda_{i}^{k} \right] \\
= \bar{X}_{i}^{k} - \frac{1}{\beta} \left[\nabla \mathcal{O}(\bar{X}_{i}^{k}) - \varrho(\bar{X}_{i}^{k+1} - \bar{X}_{i}^{k}) - \lambda_{i}^{k+1} \right], \quad (14)$$

with β determining the strength of regularization. The change of \mathcal{L} due to Line 5 can be bounded as follows:

Lemma 8.1: If $\nabla \mathcal{O}$ is $L_{\mathcal{O}}$ -Lipschitz continuous, then Line 5 of Algorithm 2 will monotonically increase \mathcal{L} by at most:

$$\frac{2(\beta-\varrho)^2}{\varrho} \|\bar{X}_i^{k+1} - \bar{X}_i^k\|^2 + \frac{2(\beta-\varrho+L_{\mathcal{O}})^2}{\varrho} \|\bar{X}_i^k - \bar{X}_i^{k-1}\|^2.$$

Proof: Some minor rearrangement of Equation 14 would lead to:

$$(\beta - \varrho)(\bar{X}_i^{k+1} - \bar{X}_i^k) = \lambda_i^{k+1} - \nabla \mathcal{O}(\bar{X}_i^k). \tag{15}$$

We have the following identity due to $L_{\mathcal{O}}$ -Lipschitz property of $\nabla \mathcal{O}$:

$$\begin{split} & \|\lambda_{i}^{k+1} - \lambda_{i}^{k}\| \leq \|\nabla \mathcal{O}(\bar{X}_{i}^{k}) - \nabla \mathcal{O}(\bar{X}_{i}^{k-1})\| + \\ & (\beta - \varrho) \|\bar{X}_{i}^{k+1} - \bar{X}_{i}^{k}\| + (\beta - \varrho) \|\bar{X}_{i}^{k} - \bar{X}_{i}^{k-1}\| \\ \leq & (\beta - \varrho) \|\bar{X}_{i}^{k+1} - \bar{X}_{i}^{k}\| + (\beta - \varrho + L_{\mathcal{O}}) \|\bar{X}_{i}^{k} - \bar{X}_{i}^{k-1}\|. \end{split}$$

By the inequality $(a+b)^2 \le 2a^2 + 2b^2$, we can derive the result to be proved.

Further, the change of \mathcal{L} due to Line 4 can also be bounded as follows:

Lemma 8.2: If $\nabla \mathcal{O}$ is $L_{\mathcal{O}}$ -Lipschitz continuous, then Line 4 of Algorithm 2 will monotonically increase \mathcal{L} by at most:

$$\left[\frac{L_{\mathcal{O}} + \varrho}{2} - \beta\right] \|\bar{X}_i^{k+1} - \bar{X}_i^k\|^2.$$

Proof: There are two terms related to \bar{X}_i , namely $\mathcal{O}(\bar{X}_i)$ and $\varrho/2\|\bar{X}_i(\theta^{k+1}) - \bar{X}_i - \lambda_i^k/\varrho\|^2$. Using Equation 14, the change to the first term can be bounded as:

$$\mathcal{O}(\bar{X}_{i}^{k+1}) - \mathcal{O}(\bar{X}_{i}^{k})$$

$$\leq \nabla \mathcal{O}(\bar{X}_{i}^{k})^{T}(\bar{X}_{i}^{k+1} - \bar{X}_{i}^{k}) + \frac{L_{\mathcal{O}}}{2} \|\bar{X}_{i}^{k+1} - \bar{X}_{i}^{k}\|^{2}$$

$$= \lambda_{i}^{k+1} (\bar{X}_{i}^{k+1} - \bar{X}_{i}^{k}) + \left[\frac{L_{\mathcal{O}}}{2} - (\beta - \varrho)\right] \|\bar{X}_{i}^{k+1} - \bar{X}_{i}^{k}\|^{2}.$$
(16)

The change to the second term can be bounded as:

$$\frac{\varrho}{2} \| \bar{X}_{i}(\theta^{k+1}) - \bar{X}_{i}^{k+1} - \frac{\lambda_{i}^{k}}{\varrho} \|^{2} - \frac{\varrho}{2} \| \bar{X}_{i}(\theta^{k+1}) - \bar{X}_{i}^{k} - \frac{\lambda_{i}^{k}}{\varrho} \|^{2}$$

$$= \frac{\varrho}{2} (\bar{X}_{i}^{k} - \bar{X}_{i}^{k+1})^{T} \left[\frac{-2\lambda_{i}^{k+1}}{\varrho} + \bar{X}_{i}^{k+1} - \bar{X}_{i}^{k} \right]$$

$$= -\frac{\varrho}{2} \| \bar{X}_{i}^{k+1} - \bar{X}_{i}^{k} \|^{2} - \lambda_{i}^{k+1}^{T} (\bar{X}_{i}^{k+1} - \bar{X}_{i}^{k}). \tag{17}$$

We can derive the result to be proved by summing up Equation 16 and Equation 17.

We can then establish the Lyapunov candidate $\mathcal{L}_{\kappa}^{k} \triangleq \mathcal{L}(\theta^{k+1}, \bar{X}_{i}, \lambda_{i}^{k}, n_{i}^{k}, d_{i}^{k}, n_{ij}^{k}, d_{ij}^{k}) + \kappa \|\bar{X}_{i}^{k+1} - \bar{X}_{i}^{k}\|^{2}$ and prove its monotonic property below:

Lemma 8.3: If $\nabla \mathcal{O}$ is $L_{\mathcal{O}}$ -Lipschitz continuous, then the sequence $\{\mathcal{L}_{\kappa}^k\}$ is monotonically decreasing when:

$$\varrho = \beta \quad \kappa = \beta/4 \quad \beta > 2\sqrt{2}L_{\mathcal{O}}.$$

Proof: The other parts of Algorithm 2 are monotonically decreasing $\mathcal L$ except for Line 4 and Line 5. Combining the results of Lemma 8.1 and Lemma 8.2, we have:

$$\begin{split} &\mathcal{L}_{\kappa}^{k+1} - \mathcal{L}_{\kappa}^{k} \leq \kappa \sum_{i} \|\bar{X}_{i}^{k+1} - \bar{X}_{i}^{k}\|^{2} - \kappa \sum_{i} \|\bar{X}_{i}^{k} - \bar{X}_{i}^{k-1}\|^{2} + \\ &\frac{2(\beta - \varrho)^{2}}{\varrho} \sum_{i} \|\bar{X}_{i}^{k+1} - \bar{X}_{i}^{k}\|^{2} + \frac{2(\beta - \varrho + L_{\mathcal{O}})^{2}}{\varrho} \sum_{i} \|\bar{X}_{i}^{k} - \bar{X}_{i}^{k-1}\|^{2} + \\ & \left[\frac{L_{\mathcal{O}} + \varrho}{2} - \beta \right] \sum_{i} \|\bar{X}_{i}^{k+1} - \bar{X}_{i}^{k}\|^{2} \\ &= \left[\frac{2(\beta - \varrho)^{2}}{\varrho} + \frac{L_{\mathcal{O}} + \varrho}{2} - \beta + \kappa \right] \sum_{i} \|\bar{X}_{i}^{k+1} - \bar{X}_{i}^{k}\|^{2} + \\ & \left[\frac{2(\beta - \varrho + L_{\mathcal{O}})^{2}}{\varrho} - \kappa \right] \sum_{i} \|\bar{X}_{i}^{k} - \bar{X}_{i}^{k-1}\|^{2}. \end{split}$$

It can be verified that both terms in the last equation are negative using the parameter choices give above.

Next, we show that the sequence $\{\mathcal{L}_{\kappa}^{k}\}$ is convergent:

Lemma 8.4: We denote the following remainder as \mathcal{R} :

$$\mathcal{R}(\theta, n_i, d_i, n_{ij}, d_{ij}) \triangleq \gamma \sum_{i} \left[\sum_{x \in X_i} \log(n_i x(\theta) + d_i) + \sum_{z \in Z} \log(-n_i z - d_i) \right] -$$

$$\gamma \sum_{ij} \left[\sum_{x \in X_i} \log(n_{ij}x(\theta) + d_{ij}) + \sum_{x \in X_j} \log(-n_{ij}x(\theta) - d_{ij}) \right].$$

If $\nabla \mathcal{O}$ is $L_{\mathcal{O}}$ -Lipschitz continuous, $\mathcal{R} \geq \underline{\mathcal{R}}$ and $\mathcal{O} \geq \underline{\mathcal{O}}$ are lower-bounded and parameters are chosen according to Lemma 8.3, then the Lyapunov candidate \mathcal{L}_{κ} is lower-bounded and the sequence $\{\mathcal{L}_{\kappa}^k\}$ is convergent.

Proof: We have the following result from Equation 15:

$$\mathcal{L}_{\kappa}^{k} \geq \underline{\mathcal{R}} + \sum_{i} \mathcal{O}(\bar{X}_{i}^{k}) +$$

$$\sum_{i} \frac{\varrho}{2} \|X_{i}(\theta^{k}) - \bar{X}_{i}^{k}\|^{2} + \lambda_{i}^{kT} (X_{i}(\theta^{k}) - \bar{X}_{i}^{k})$$

$$= \underline{\mathcal{R}} + \sum_{i} \mathcal{O}(\bar{X}_{i}^{k}) + \nabla \mathcal{O}(\bar{X}_{i}^{k})^{T} (X_{i}(\theta^{k}) - \bar{X}_{i}^{k}) +$$

$$\sum_{i} \frac{\varrho}{2} \|X_{i}(\theta^{k}) - \bar{X}_{i}^{k}\|^{2} + (\beta - \varrho)(\bar{X}_{i}^{k+1} - \bar{X}_{i}^{k})^{T} (X_{i}(\theta^{k}) - \bar{X}_{i}^{k})$$

$$\geq \underline{\mathcal{R}} + \sum_{i} \mathcal{O}(X_{i}(\theta^{k})) - \frac{L_{\mathcal{O}}}{2} \|X_{i}(\theta^{k}) - \bar{X}_{i}^{k}\|^{2} +$$

$$\sum_{i} \frac{\varrho}{2} \|X_{i}(\theta^{k}) - \bar{X}_{i}^{k}\|^{2} + (\beta - \varrho)(\bar{X}_{i}^{k+1} - \bar{X}_{i}^{k})^{T} (X_{i}(\theta^{k}) - \bar{X}_{i}^{k})$$

$$\geq \underline{\mathcal{R}} + \sum_{i} \underline{\mathcal{O}} + \frac{\varrho - L_{\mathcal{O}}}{2} \|X_{i}(\theta^{k}) - \bar{X}_{i}^{k}\|^{2} \geq \underline{\mathcal{R}} + \sum_{i} \underline{\mathcal{O}},$$

so the sequence $\{\mathcal{L}_{\kappa}^k\}$ is monotonically decreasing, lower-bounded, and thus convergent.

Remark 8.5: If time optimality is considered, then Lemma 8.3 holds with the following choice of remainder:

$$\mathcal{R}(\theta, \Delta t, n_i, d_i, n_{ij}, d_{ij}) \triangleq w \Delta t - \gamma \sum_{i} \log(v_{\text{max}} \Delta t - ||V_i||) - \gamma \sum_{i} \log(a_{\text{max}} \Delta t^2 - ||A_i||) - \gamma \sum_{i} \left[\sum_{x \in X_i} \log(n_i x(\theta) + d_i) + \sum_{z \in Z} \log(-n_i z - d_i) \right] - \gamma \sum_{ij} \left[\sum_{x \in X_i} \log(n_{ij} x(\theta) + d_{ij}) + \sum_{x \in X_j} \log(-n_{ij} x(\theta) - d_{ij}) \right].$$

Next, we establish the convergence guarantee for a convergent sub-sequence. The first-order critical point should satisfy the following conditions:

$$\left\| \frac{\partial \mathcal{L}}{\partial \lambda_i} \right\| = \|X_i(\theta) - \bar{X}_i\| = 0 \tag{18}$$

$$\left\| \frac{\partial \mathcal{L}}{\partial \bar{X}_{\cdot}} \right\| = \left\| \nabla \mathcal{O}(\bar{X}_{i}) - \lambda_{i} \right\| = 0 \tag{19}$$

$$\|\nabla \mathcal{L} \circ \exp\left(\Theta, \exp_{n_i}(0), d_i, \exp_{n_{ij}}(0), d_{ij}\right)\| = 0,$$
 (20)

where we define $\mathcal{L} \circ \exp$ with each n_i (w.r.t. n_{ij}) replaced by $\exp_{n_i}(v_i)$ (w.r.t. $\exp_{n_{ij}}(v_{ij})$).

Lemma 8.6: If $\nabla \mathcal{O}$ is $L_{\mathcal{O}}$ -Lipschitz continuous, both \mathcal{R} and \mathcal{O} are lower-bounded and parameters are chosen according to Lemma 8.3, then every accumulation point of the sequence $\{(\Theta^k, \bar{X}_i^k, P_i^k, P_{ij}^k)\}$ generated by Algorithm 2 is a critical

point. Suppose the sequence is convergent, the local convergence speed of $\|\nabla \mathcal{L} \circ \exp\|$ is $\mathcal{O}(1/\sqrt{K})$.

Proof: The sequence $\{\mathcal{L}_{\kappa}\left(\Theta^{k}, \bar{X}_{i}^{k}, \lambda_{i}^{k}, P_{i}^{k}, P_{ij}^{k}\right)\}$ is convergent due to Lemma 8.4. We assume the accumulation point is $\left(\bar{\Theta}, \bar{X}_{i}, \bar{P}_{i}, \bar{P}_{ij}\right)$ with convergent sub-sequence identified by the index subset: $\mathcal{K} \subset \{k|k=1,2,\cdots\}$.

Applying Lemma 7.1 and Lemma 8.3: The reduction of \mathcal{L}_{κ} over one iteration of Algorithm 2 can be bounded as:

$$\mathcal{L}_{\kappa}^{k+1} + c \|\Theta^{k+1} - \Theta^{k}\|^{2} + c \sum_{i} \|v_{i}^{k}\|^{2} + \|d_{i}^{k+1} - d_{i}^{k}\|^{2} + c \sum_{ij} \|v_{ij}^{k}\|^{2} + \|d_{ij}^{k+1} - d_{ij}^{k}\|^{2} - \left[\frac{2(\beta - \varrho)^{2}}{\varrho} + \frac{L_{\mathcal{O}} + \varrho}{2} - \beta + \kappa\right] \sum_{i} \|\bar{X}_{i}^{k+1} - \bar{X}_{i}^{k}\|^{2} - \left[\frac{2(\beta - \varrho + L_{\mathcal{O}})^{2}}{\varrho} - \kappa\right] \sum_{i} \|\bar{X}_{i}^{k} - \bar{X}_{i}^{k-1}\|^{2} \le \mathcal{L}_{\kappa}^{k}, \tag{21}$$

from which we conclude that $\lim_{k\to\infty}\|\Theta^{k+1}-\Theta^k\|=0$, $\lim_{k\to\infty}\|v^k\|=0$, and $\lim_{k\to\infty}\|d^{k+1}-d^k\|=0$ for any P, and $\lim_{k\to\infty}\|\bar{X}_i^{k+1}-\bar{X}_i^k\|=0$. Equation 20 is satisfied at the accumulation point following the same reasoning as Lemma 7.2. Taking limits on both sides of Equation 15 and we have:

$$\begin{split} & \lim_{k \to \infty} \| \boldsymbol{\lambda}^{k+1} - \nabla \mathcal{O}(\bar{X}_i^{k+1}) \| \\ & \leq \lim_{k \to \infty} \| \boldsymbol{\lambda}^{k+1} - \nabla \mathcal{O}(\bar{X}_i^{k}) \| + \| \nabla \mathcal{O}(\bar{X}_i^{k+1}) - \nabla \mathcal{O}(\bar{X}_i^{k}) \| \\ & \leq L_{\mathcal{O}} \lim_{k \to \infty} \| \bar{X}_i^{k+1} - \bar{X}_i^{k} \| = 0, \end{split}$$

from which Equation 19 follows. We then take limits on both sides of Line 5 and we have $\lim_{k\to\infty}\|X_i(\theta^k)-\bar{X}_i^k\|=0$, from which Equation 18 follows.

Convergence Speed: Summing up Equation 21 over K iterations and we have:

$$\begin{split} K \min_{k=1,\cdots,K} \left[\| \bar{X}_i^{k+1} - \bar{X}_i^k \|^2 + \| \bar{X}_i^k - \bar{X}_i^{k-1} \|^2 \right] \\ \leq & \frac{\mathcal{L}_{\kappa}^1 - \underline{\mathcal{L}}_{\kappa}}{\min\left(-\left\lceil \frac{2(\beta-\varrho)^2}{\varrho} + \frac{L_{\mathcal{O}} + \varrho}{2} - \beta + \kappa \right\rceil, -\left\lceil \frac{2(\beta-\varrho+L_{\mathcal{O}})^2}{\varrho} - \kappa \right\rceil \right)}. \end{split}$$

We plug these results into Equation 14 and Lemma 8.1 to derive:

$$\begin{split} &\|X_{i}(\theta^{k+1}) - \bar{X}_{i}^{k+1}\|^{2} = \frac{1}{\varrho^{2}} \|\lambda_{i}^{k+1} - \lambda_{i}^{k}\|^{2} \\ &\leq \frac{2(\beta - \varrho)^{2}}{\varrho^{2}} \|\bar{X}_{i}^{k+1} - \bar{X}_{i}^{k}\|^{2} + \frac{2(\beta - \varrho + L_{\mathcal{O}})^{2}}{\varrho^{2}} \|\bar{X}_{i}^{k} - \bar{X}_{i}^{k-1}\|^{2} \\ &\leq \frac{\max(2(\beta - \varrho)^{2}, 2(\beta - \varrho + L_{\mathcal{O}})^{2})}{\varrho^{2}} \left[\|\bar{X}_{i}^{k+1} - \bar{X}_{i}^{k}\|^{2} + \|\bar{X}_{i}^{k} - \bar{X}_{i}^{k-1}\|^{2} \right] \\ &\|\lambda_{i}^{k} - \nabla \mathcal{O}(\bar{X}_{i}^{k})\|^{2} \leq 2\|\lambda_{i}^{k+1} - \nabla \mathcal{O}(\bar{X}_{i}^{k})\|^{2} + 2\|\lambda_{i}^{k+1} - \lambda_{i}^{k}\|^{2} \\ &\leq 4(\beta - \varrho)^{2} \|\bar{X}_{i}^{k+1} - \bar{X}_{i}^{k}\|^{2} + 2(\beta - \varrho + L_{\mathcal{O}})^{2} \|\bar{X}_{i}^{k} - \bar{X}_{i}^{k-1}\|^{2} \\ &\leq \max(4(\beta - \varrho)^{2}, 2(\beta - \varrho + L_{\mathcal{O}})^{2}) \left[\|\bar{X}_{i}^{k+1} - \bar{X}_{i}^{k}\|^{2} + \|\bar{X}_{i}^{k} - \bar{X}_{i}^{k-1}\|^{2} \right], \end{split}$$

which establishes the $\mathcal{O}(1/\sqrt{K})$ convergence speed of Equation 18 and Equation 19. The local convergence speed of Equation 20 follows the same reasoning as Lemma 7.2. Finally, we establish whole sequence convergence and thus local convergence speed assuming KŁ property of $\mathcal{L} \circ \exp$.

Lemma 8.7: If $\nabla \mathcal{O}$ is $L_{\mathcal{O}}$ -Lipschitz continuous, \mathcal{R} and \mathcal{O} are lower-bounded and pertains the KŁ property (Definition 7.3), and the sequence $\{\left(\Theta^k, \bar{X}_i^k, P_i^k, P_{ij}^k\right)\}$ generated by Algorithm 2 has a finite accumulation point, then the sequence

is convergent.

Proof: We denote $(\bar{\Theta}, \bar{X}_i, \bar{\lambda}_i, \bar{P}_i, \bar{P}_{ij})$ as the accumulation point. By invoking Lemma 8.6, we know that $\nabla \mathcal{L} \circ \exp = 0$. W.l.o.g., we assume $\mathcal{L}(\bar{\Theta}, \bar{X}_i, \bar{\lambda}_i, \bar{P}_i, \bar{P}_{ij}) = 0$. By continuity, we can choose a small neighborhood $B_{2\rho} \subset \text{dom} \mathcal{L}$ where $\|\nabla \mathcal{L} \circ \exp\| < \epsilon$ and the the KŁ property holds. We further denote $\nabla \mathcal{L} \circ \exp$ as L-Lipschitz continuous and every X_i is L_{X_i} -Lipschitz continuous within $B_{2\rho}$. Finally, in a sufficiently small local neighborhood, we can setup strong equivalence between metrics in tangent space and ambient space for any point in $B_{2\rho}$. If we start from $(\Theta^k, \bar{X}_i^k, \lambda_i^k, P_i^k, P_{ij}^k) \in B_{\rho}$, we choose sufficiently large k_0 such that the subsequent point $(\Theta^{k+1}, \bar{X}_i^{k+1}, \lambda_i^{k+1}, P_i^{k+1}, P_{ij}^{k+1}) \in B_{2\rho}$ for every $k \geq k_0$ due to Lemma 7.2. W.l.o.g., we can assume $k_0 = 0$. Since there is a sub-sequence converging to $(\bar{\Theta}, \bar{X}_i, \bar{\lambda}_i, \bar{P}_i, \bar{P}_{ij})$, we can choose large enough $k \geq k_0$ (W.l.o.g., we can assume $k_0 = 0$) so that:

$$\left(\Theta^{0}, \bar{X}_{i}^{0}, \lambda_{i}^{0}, P_{i}^{0}, P_{ij}^{0}\right) \in B_{\rho - L_{1}/L_{2}\phi(\mathcal{L}\left(\Theta^{0}, \bar{X}_{i}^{0}, \lambda_{i}^{0}, P_{i}^{0}, P_{ij}^{0}\right)}. \tag{22}$$

Next, we show that every subsequent point $(\Theta^k, \bar{X}_i^k, \lambda_i^k, P_i^k, P_{ij}^k) \in B_\rho$ lies in by induction. If we already have this property for all previous points, i.e., $(\Theta^0, \bar{X}_i^0, \lambda_i^0, P_i^0, P_{ij}^0), \cdots, (\Theta^k, \bar{X}_i^k, \lambda_i^k, P_i^k, P_{ij}^k) \in B_\rho$, then the following holds for $(\Theta^{k+1}, \bar{X}_i^{k+1}, \lambda_i^{k+1}, P_i^{k+1}, P_{ij}^{k+1}) \in B_\rho$:

$$\begin{split} & \frac{\mathcal{L}\left(\Theta^{k}, \bar{X}_{i}^{k}, \lambda_{i}^{k}, P_{i}^{k}, P_{ij}^{k}\right) - \mathcal{L}\left(\Theta^{k+1}, \bar{X}_{i}^{k+1}, \lambda_{i}^{k+1}, P_{i}^{k+1}, P_{ij}^{k+1}\right)}{\phi(\mathcal{L}\left(\Theta^{k}, \bar{X}_{i}^{k}, \lambda_{i}^{k}, P_{i}^{k}, P_{ij}^{k}\right)) - \phi(\mathcal{L}\left(\Theta^{k+1}, \bar{X}_{i}^{k+1}, \lambda_{i}^{k+1}, P_{i}^{k+1}, P_{ij}^{k+1}\right))} \\ \leq & 1/\phi'(\mathcal{L}\left(\Theta^{k}, \bar{X}_{i}^{k}, \lambda_{i}^{k}, P_{ij}^{k}\right)) \\ \leq & \|\nabla \mathcal{L}(\Theta^{k}, \bar{X}_{i}^{k}, \lambda_{i}^{k}, \exp_{n_{i}^{k}}(0), d_{i}^{k}, \exp_{n_{i}^{k}}(0), d_{ij}^{k})\| \\ = & \Delta + \sum_{i} \|\varrho(\bar{X}_{i}^{k} - X_{i}(\theta^{k})) + \nabla \mathcal{O}(\bar{X}_{i}^{k}) - \lambda_{i}^{k}\| + \sum_{i} \|X_{i}(\theta^{k}) - \bar{X}_{i}^{k}\| \\ \leq & \Delta + \sum_{i} \|\nabla \mathcal{O}(\bar{X}_{i}^{k}) - \lambda_{i}^{k+1} + \lambda_{i}^{k+1} - \lambda^{k}\| + (\varrho + 1)\|X_{i}(\theta^{k}) - \bar{X}_{i}^{k}\| \\ \leq & \Delta + \sum_{i} \|\lambda_{i}^{k+1} - \lambda^{k}\| + (\beta - \varrho)\|\bar{X}_{i}^{k+1} - \bar{X}_{i}^{k}\| + (\varrho + 1)\|X_{i}(\theta^{k}) - \bar{X}_{i}^{k}\| \\ \leq & \Delta + \sum_{i} \|\lambda_{i}^{k+1} - \lambda^{k}\| + (\beta - \varrho)\|\bar{X}_{i}^{k+1} - \bar{X}_{i}^{k}\| + (\varrho + 1)\|X_{i}(\theta^{k}) - \bar{X}_{i}^{k}\| \\ \leq & \Delta + \sum_{i} \|\lambda_{i}^{k+1} - \lambda^{k}\| + (\beta - \varrho)\|\bar{X}_{i}^{k+1} - \bar{X}_{i}^{k}\| + (\varrho + 1)\|X_{i}(\theta^{k}) - \bar{X}_{i}^{k}\| \\ \leq & \Delta + \sum_{i} \|\lambda_{i}^{k+1} - \lambda^{k}\| + (\beta - \varrho)\|\bar{X}_{i}^{k+1} - \bar{X}_{i}^{k}\| + (\varrho + 1)\|\bar{X}_{i}^{k+1} - \bar{X}_{i}^{k}\| \right] \\ \leq & \Delta + \sum_{i} \frac{2\varrho + 1}{\varrho} \|\lambda_{i}^{k+1} - \lambda^{k}\| + (\varrho + 1)L_{X_{i}}\|\Theta_{i}^{k+1} - \Theta^{k}\| \\ \leq & L_{1} \|\left(\Theta^{k+1}, \bar{X}_{i}^{k+1}, \lambda_{i}^{k+1}, P_{i}^{k+1}, P_{i}^{k+1}, P_{i}^{k+1}\right) - (\Theta^{k}, \bar{X}_{i}^{k}, \lambda_{i}^{k}, P_{i}^{k}, P_{ij}^{k}\right) \|, \end{split}$$

where we define:

$$\begin{split} \Delta &\triangleq \left[\frac{L}{2\gamma(1-c)} + \sum_{i} L + \sum_{ij} L\right] \|\Theta^{k+1} - \Theta^{k}\| + \\ &\frac{L\bar{L}}{2\gamma(1-c)} \left[\sum_{i} \|P_{i}^{k+1} - P_{i}^{k}\| + \sum_{ij} \|P_{ij}^{k+1} - P_{ij}^{k}\|\right] \\ L_{1} &= \max\left(\frac{L}{2\gamma(1-c)} + \sum_{i} L + \sum_{ij} L + (\varrho + 1)\sum_{i} L_{X_{i}}}{\max\left(\frac{L\bar{L}}{2\gamma(1-c)}, \beta + 1, \frac{2\varrho + 1}{\varrho}\right)}\right). \end{split}$$

We have used Equation 14 in the forth inequality and the L_{X_i} -Lipschitz smoothness in the sixth inequality. We further have the following estimate of function decrease due to Lemma 8.6:

$$\begin{split} &\mathcal{L}\left(\Theta^{k},P_{i}^{k},P_{ij}^{k}\right)-\mathcal{L}\left(\Theta^{k+1},P_{i}^{k+1},P_{ij}^{k+1}\right)\\ \geq &c\|\Theta^{k+1}-\Theta^{k}\|^{2}+c\underline{L}^{2}\sum_{i}\|n_{i}^{k+1}-n_{i}^{k}\|^{2}+c\sum_{i}\|d_{i}^{k+1}-d_{i}^{k}\|^{2}+\\ &c\underline{L}^{2}\sum_{ij}\|n_{ij}^{k+1}-n_{ij}^{k}\|^{2}+c\sum_{ij}\|d_{ij}^{k+1}-d_{ij}^{k}\|^{2}-\\ &\left[\frac{2(\beta-\varrho)^{2}}{\varrho}+\frac{L_{\mathcal{O}}+\varrho}{2}-\beta+\kappa\right]\|\bar{X}_{i}^{k+1}-\bar{X}_{i}^{k}\|^{2}-\\ &\left[\frac{2(\beta-\varrho+L_{\mathcal{O}})^{2}}{\varrho}-\kappa\right]\|\bar{X}_{i}^{k}-\bar{X}_{i}^{k-1}\|^{2}\\ \geq &L_{2}\|\left(\Theta^{k+1},\bar{X}_{i}^{k+1},\lambda_{i}^{k+1},P_{i}^{k+1},P_{ij}^{k+1}\right)-\left(\Theta^{k},\bar{X}_{i}^{k},\lambda_{i}^{k},P_{i}^{k},P_{ij}^{k}\right)\|^{2}, \end{split}$$

where we define:

$$\begin{split} L_2 = \min \left(-\frac{\min(c, c\underline{L}^2)}{-\left[\frac{2(\beta-\varrho)^2}{\varrho} + \frac{L_{\mathcal{O}} + \varrho}{2} - \beta + \kappa\right]} - \left[\frac{2(\beta-\varrho+L_{\mathcal{O}})^2}{\varrho} - \kappa\right] \right). \end{split}$$

The remaining argument is identical to Lemma 7.4.